FEDERAL UNIVERSITY OF TECHNOLOGY - PARANA
GRADUATE PROGRAM IN ELECTRICAL AND COMPUTER ENGINEERING

FELIPE DE ASSIS DIAS

INCREASING IMAGE RESOLUTION FOR WIRE-MESH SENSOR BASED ON STATISTICAL RECONSTRUCTION

MASTER THESIS

CURITIBA

2017

UNIVERSIDADE TECNOLÓGICA FEDERAL DO PARANÁ
PROGRAMA DE PÓS-GRADUAÇÃO EM ENGENHARIA ELÉTRICA E INFORMÁTICA INDUSTRIAL

FELIPE DE ASSIS DIAS

AUMENTO DE RESOLUÇÃO DE IMAGEM DE SENSORES WIRE-MESH BASEADO EM RECONSTRUÇÃO ESTATÍSTICA

DISSERTAÇÃO DE MESTRADO

CURITIBA

2017

FELIPE DE ASSIS DIAS

INCREASING IMAGE RESOLUTION FOR WIRE-MESH SENSOR BASED ON STATISTICAL RECONSTRUCTION

Master thesis presented to the Graduate Program in Electrical and Computer Engineering (CPGEI) of Federal University of Technology – Paraná (UTFPR), in partial fulfilment of the requirements for the degree of Master of Science (M.Sc.).

Advisor: Prof. Dr. Marco José da Silva.

Co-Advisor: Prof. Dr. Daniel Rodrigues Pipa

CURITIBA
2017

Dados Internacionais de Catalogação na Publicação

D541in 2017

Dias, Felipe de Assis
Increasing image resolution for wire-mesh sensor based on statistical reconstruction = Aumento de resolução de imagem de sensores wire-mesh baseado em reconstrução estatística / Felipe de Assis Dias.-- 2017.
68 f.: il.; 30 cm.

Disponível também via World Wide Web.
Texto em inglês com resumo em português.
Dissertação (Mestrado) - Universidade Tecnológica Federal do Paraná. Programa de Pós-graduação em Engenharia Elétrica e Informática Industrial. Área de Concentração: Engenharia de Automação e Sistemas, Curitiba, 2017.
Bibliografia: f. 67-68.

1. Escoamento multifásico. 2. Detectores. 3. Malha de eletrodos. 4. Problemas inversos (Equações diferenciais). 5. Reconstrução de imagens. 6. Processamento de imagens - Métodos estatísticos. 7. Estatística matemática. 8. Métodos de simulação. 9. Engenharia elétrica - Dissertações. I. Silva, Marco José da, orient. II. Pipa, Daniel Rodrigues, coorient. III. Universidade Tecnológica Federal do Paraná. Programa de Pós-Graduação em Engenharia Elétrica e Informática Industrial. IV. Título. V. Título: Aumento de resolução de imagem de sensores wire-mesh baseado em reconstrução estatística.

CDD: Ed. 22 -- 621.3

Biblioteca Central do Câmpus Curitiba - UTFPR

Ministério da Educação
Universidade Tecnológica Federal do Paraná
Diretoria de Pesquisa e Pós-Graduação

TERMO DE APROVAÇÃO DE DISSERTAÇÃO Nº765

A Dissertação de Mestrado intitulada **"Increasing Image Resolution for Wire-Mesh Sensor Based on Statistical Reconstruction"** defendida em sessão pública pelo(a) candidato(a) **Felipe de Assis Dias**, no dia 04 de agosto de 2017, foi julgada para a obtenção do título de Mestre em Ciências, área de concentração Engenharia de Automação e Sistemas, e aprovada em sua forma final, pelo Programa de Pós-Graduação em Engenharia Elétrica e Informática Industrial

BANCA EXAMINADORA:

Prof(a). Dr(a). Marco José da Silva - Presidente – (UTFPR)
Prof(a). Dr(a). André Eugênio Lazzaretti - (UTFPR)
Prof(a). Dr(a). Silvio de Barros Melo – (UFPE)

A via original deste documento encontra-se arquivada na Secretaria do Programa, contendo a assinatura da Coordenação após a entrega da versão corrigida do trabalho.

Curitiba, 04 de agosto de 2017.

This thesis is dedicated to my parents and my wife.

.

Acknowledgements

I would like to thank my thesis advisor and co-advisor Prof. Dr. Marco José da Silva and Prof. Dr. Daniel Rodrigues Pipa, respectively, for the support of my investigation. They gave me the opportunity to develop research in the fields of multiphase flow and image reconstruction technique, sharing essential knowledge and insights through intense discussions. Besides this, both steered me the right direction whenever I needed it.

I would also like to thank my lab-mates, Eduardo Nunes, Aluísio Wrasse, Tiago Vendrusculo, Gabriel Torelli, Jean Longo and all other experts who were involved in the experimental or theoretical parts of this research.

I also express my gratitude to all of the Department faculty members and experts of the research group NUEM for their support.

I must express my gratitude to my parents Regina and Paulo and to my wife Esther for providing my support and continuous encouragement through the process of researching and writing this thesis. This accomplishment would not have been possible without them.

Finally, I would like to acknowledge to the Brazilian National Council for Scientific and Technological Development (CNPq) and FUNTEF-PR for the financial support.

Curitiba, July 2017. Felipe de Assis Dias

Abstract

DIAS, F. A., **Increasing Image Resolution for Wire-Mesh Sensor Based on Statistical Reconstruction.** 68 p. Master Thesis – Graduate Program in Electrical and Computer Engineering (CPGEI), Federal University of Technology – Paraná (UTFPR). Curitiba, 2015.

Wire-mesh sensors (WMS) are able to generate cross-sectional images of multiphase flow and have been widely used to investigate flow phenomena in pilot plant studies. Such devices are able to measure flow parameters such as phase fraction (e.g. gas/liquid fraction) distribution and visualize multiphase flows with high temporal and spatial resolution. Hence, being important tool for detailed flow investigation. However, its sensing principle is based on intrusive electrodes placed inside the pipe where a multiphase flow streams. The image resolution generated by the sensor is given by the number of crossing points formed by the transmitter and receptor wires. In many processes, however, the intrusive effect of such sensor might be a limitation on its use. Therefore, a reduced number of wires could possibly increase the application field of wire-mesh sensors. For this reason, the present work presents an image reconstruction method to increase resolution of WMS data with less than optimal number of electrode wires. In this way, a reduction of intrusive effects on the process under investigation may be achieved. The reconstruction method is based on statistical view of regularization and is known as Maximum a Posterior (MAP). 16x16 WMS flow data are used to determine a Multivariate Gaussian flow model, which in turn is used as regularization in the reconstruction. A sensitive matrix is estimated by finite element method (FEM) to incorporate MAP algorithm. Experimental data are used to validate the proposed method, which is compared with spline interpolation. Experimental results show that the MAP reconstruction performs better than interpolation and achieves deviation in gas void fraction estimation in the range of $\pm 10\%$ in the vast majority of operating points. The tests were performed in a horizontal water-gas flow loop operating at intermittent (slug) flow regime.

Keywords: Wire-mesh sensor; Multiphase flow; Inverse Problem; Statistical Image Reconstruction; Maximum a Posteriori (MAP).

Resumo

DIAS, F. A., **Aumento de Resolução de Imagens de Sensores Wire-Mesh Baseado em Reconstrução Estatística.** 68 p. Dissertação de Mestrado – Pós-Graduação em Engenharia Elétrica e Informática Industrial (CPGEI), Universidade Tecnológica Federal do Paraná (UTFPR). Curitiba, 2017.

Sensores wire-mesh (WMS) são capazes de gerar imagens da seção transversal de escoamentos multifásicos e tem sido amplamente utilizados para investigar fenômenos de escoamentos em plantas piloto. Tais dispositivos são capazes de medir parâmetros de escoamento tais como distribuição da fração de fase (por exemplo fração de gás ou líquido) e visualizar escoamentos multifásicos com alta resolução temporal e espacial. Sendo portanto, uma ferramenta importante para investigações de escoamentos mais detalhadas. No entanto, seu princípio de medição é baseado em eletrodos intrusivos posicionados dentro do tubo onde o escoamento flui. A resolução da imagem gerada pelo sensor é dada pelo número de cruzamentos entre os fios transmissores e receptores. Em muitos processos, no entanto, efeitos de intrusividade de tal sensor pode ser uma limitação no seu uso. Por isso, um número reduzido de fios poderia permitir uma expansão do campo de aplicações do sensor *wire-mesh*. Por essa razão, o presente trabalho sugere um método de reconstrução de imagem para aumentar a resolução dos dados de um sensor *wire-mesh* com um número de eletrodos menor que o ótimo. Desta forma, os efeitos de intrusividade no processo investigado poderiam ser reduzidos. O método de reconstrução é baseado em uma abordagem estatística de regularização e é conhecido como *Maximum a Posteriori* (MAP). Dados de escoamento de um WMS 16x16 são usados para determinar um modelo gaussiano multivariável do escoamento, o qual são empregados como regularização na reconstrução. Uma matriz de sensitividade é estimada pelo método de elementos finitos (FEM) para incorporar o algoritmo MAP. Dados experimentais são usados para validar o método proposto, sendo comparado com interpolação do tipo *spline*. Resultados experimentais mostram que a reconstrução por MAP possui um desempenho melhor do que interpolação do tipo *spline*, alcançando desvios de fração de vazio dentro de uma faixa de $\pm$ 10% na grande maioria dos pontos de operação. A validação foi executada em um loop de escoamento horizontal água/gás em regime intermitente (golfada).

Palavras-chave: Sensor *Wire-mesh*; Escoamento multifásico; Problemas inversos; Reconstrução de imagens estatística; Máximum a Posteriori (MAP).

Contents

List of figures

List of tables

Nomenclature

Roman symbols

A	Area	m^2
C	Capacitance	F
C_{sim}	Capacitance simulated	F
D	Pipe diameter / Domain	mm / -
d_w	Distance between electrode wires	mm
d_z	Axial distance between WMS planes	mm
$\mathbf{f}$	WMS image	-
$\hat{\mathbf{f}}$	Reconstructed image	-
g	Gravity acceleration vector	m/s^2
G	Gas phase	-
$\mathbf{g}$	observation/acquisition data	-
$\mathbf{H}$	Sensitivity map	-
i, j	Spatial indeces	-
J	Superficial velocity	m/s
K	Position	-
k	Constant	-
L	Length	mm
P	Phase indicator	-
$\boldsymbol{r}$	position vector	m
$\mathbf{S}$	Subsampling operator	-
t	time	t

V	Voltage	V
$\mathbf{x}$	spatial position	m
$\boldsymbol{W}$	Sensitivity map	-

Greek symbols

Λ	Specific admittance	S
α	Phase/Void fraction	m^2
δ	Relative deviation from a reference value	-
ε	Electric permittivity	-
σ	Variance	-
ρ	Electric charge density	C/m^3
Γ	Wire boundaries	-
Υ	Gaussian white noise	-

Subscripts

A	Air
B, b	Bubble
g	Gas
H	High
i	Initial
i	Input
L	Low
o	Output
P	Phase

S	Slug
T	Total
W, w	Water
x	Unknown

Abbreviations

CGLS	Conjugate gradient
DB	Dispersed bubble
FEM	Finite element method
HR	High resolution
HZDR	Helmholtz-Zentrum Dresden-Rossendorf
I	Intermittent flow
LASII	Laboratório de Sensores e Instrumentação Industrial
LBP	Linear back projection
LR	Low resolution
LRDWT	Low resolution data without treatment
MAP	Maximum a Posteriori
MFM	Multiphase flow metering
MGFM	Multivariable Gaussian flow model
MSE	Mean Squared Error
MVD	Mean void fraction
PCB	Printed circuit board
PDE	Partial differential equation
PSF	Point-spread function
RMS	Root Mean Square

SD	Standard deviation
SF	Stratified flow
SW	Stratified wavy flow
UTFPR	Universidade Tecnológica Federal do Paraná
VF	Void Fraction
VFD	Void fraction deviation
VFE	Void fraction error
WMS	Wire-mesh Sensor

Chapter 1

Introduction

In this Chapter, we present the motivation and objectives of the thesis as well as summarizes the organization of the work.

1.1 Motivation

Multiphase flows are found in several industrial processes from different fields, i.e., chemical, nuclear, mechanical, petroleum engineering, etc. In the case of petroleum industry, multiphase flow is commonly confined to pipes and occurs as gas-oil flow for instance in productions and transportation lines. The monitoring of parameters in multiphase flow such as phase fraction (i.e. gas void fraction or liquid holdup) are desired, since such flows often determine the safety and efficiency of plants and processes (Falcone, 2002). For this reason, great effort has been employed to design and improve multiphase-flow-metering (MFM) systems able to measure two or more phases simultaneously, i.e. without the need to previous phase separation (Falcone, 2009). Here, a cost-benefit analysis should be performed, because instruments dedicated to multiphase flow metering may reduce operational cost and time processing while the measurement uncertainty is increased in relationship to single-phase sensors (NSOGM Handbook of Multiphase Flow Metering, 2005).

Quite often, pilot plant studies are required in order to investigate detailed flow behavior and hence advanced flow instrumentation is sought. In this way, researchers have been employed multiphase flow sensors to carry out experiments in order to develop and evaluate mathematical models and numerical codes, as well as to better understand such phenomena

(Bertola, 2003). A wide variety of industrial sensors has been developed, e.g. tomographic sensors based on gamma-ray, x-ray, ultrasound, electrical impedance/capacitance, etc (for an overview see Da Silva (2008)).

In the class of sensors based on electrical impedance/capacitance technology, wire-mesh sensor (WMS) has been successfully applied for better understand of multiphase flow phenomena (Prasser, 2008). Results of such surveys are enabling the improvement of models and prediction tools by experimental data using WMS.

Although the sensor has sufficiently high temporal and spatial resolution, its architecture is based on intrusive electrodes. That is, the sensor is built by a number of thin stainless steel wires stretched over the pipe cross section. The image resolution generated by the sensor is given by the number of crossing points of transmitter and receptor wires. In many processes, however, the intrusive effect of such sensor might be a limitation on its use. Therefore, a reduced number of wires could possibly increase the application field of wire-mesh sensors. In this way, few works contributed to improve resolution of WMS. Da Silva (2008) and Wagner (2008) investigated the spatial sensitivity distribution of WMS using numerical field simulation. However, no reconstruction method was employed. Studies by Sun (2011) and Weimin (2016) presented numerical simulation using reconstruction image based on inverse problems in order to increase resolution of WMS with optimal electrode wires. Both researchers employed classical algorithms, i.e. *conjugate gradient* (CGLS), *linear back projection* (LBP), *Landweber iteration* and *total variation*. Results of both works provided better image resolution than simple interpolation, but intrusive effects remain unchanged.

In that context, the present thesis presents a reconstruction technique using statistical view of regularization to improve void fraction measurement and image resolution from a sensor with less than optimal electrodes number. As rule of thumb in earlier studies, a spatial resolution of 2-3 mm has been frequently used (Prasser, 2008). For instance, for one-inch pipe, traditionally a 16x16 sensor has been applied. Thus, in this work we reduced the number of the one-inch sensor to 8x8, 6x6, 4x4 and 2x2 wire configurations. The aim is to reduce intrusive effects and to propose an image reconstruction approach, which may improve both final image resolution and the derived parameter: cross-sectional averaged void fraction (α_{cs}).

1.2 Problem statement

In order to illustrate the problem of reducing the number of electrodes and subsequent application of an algorithm to recover the image resolution to commonly applied values, Figure 1.1 shows the process of decreasing by a factor of two the number of electrodes for an one-inch WMS. To model the direct problem, i.e. conversion of 16x16 measurements to lower resolutions, we employed Finite Element Methods (FEM) to obtain the electrical field distributions and the sensor readings. From this process, a so-called sensitivity matrix is obtained (see section 3.2.2 for details). A sensitivity matrix is an operator that includes point-spread function (PSF) as well as the subsampling function. However, when such simple operator it is used by conventional inverse problem algorithms such as *linear back projection* and *minimum-norm*, inadequate results are obtained as illustrated in Figure 1.1.

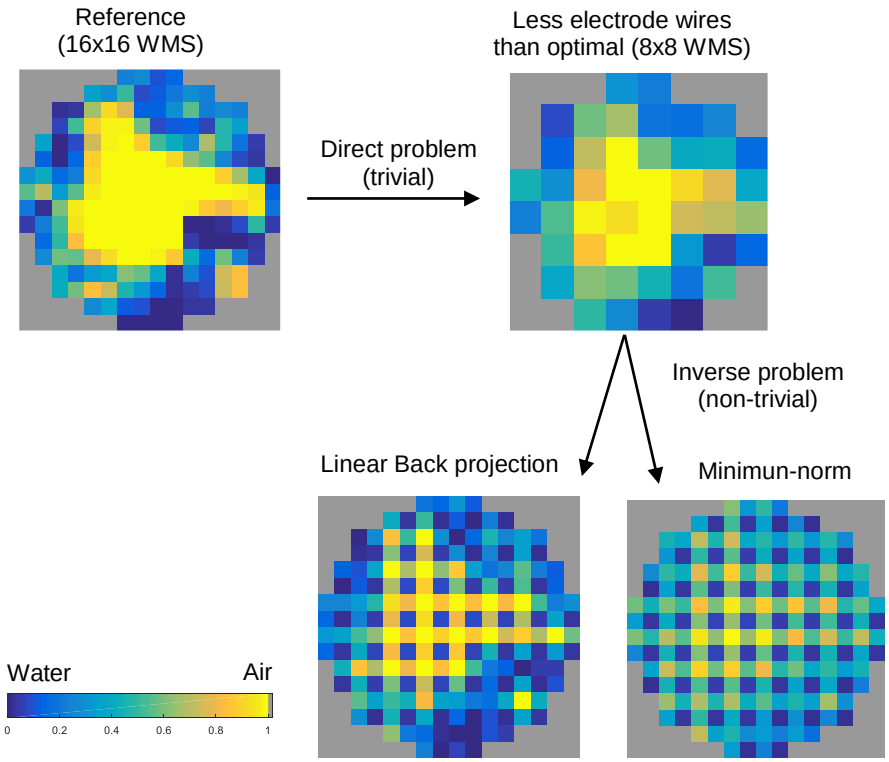

Figure 1.1: Direct and inverse problem results. Grey, yellow and blue pixels are border of the pipe, gas and water phases, respectively.

This occurs because the inverse problem applied in wire-mesh sensors with less electrode wires than optimal is highly undetermined. Therefore, we used real 16x16 WMS flow data to determine a Multivariate Gaussian Flow Model (MGFM), which in then is used as *a priori* knowledge (regularization) in the reconstruction. This approach is based on the optimization problem known as *Maximum a posteriori* (MAP).

In order to validate the MAP algorithm, a set of experiments was carried out in a horizontal liquid-gas flow loop. The superficial velocity of water and gas phases were tuned into a range of slug flow pattern. The experimental data were reconstructed by MAP and compared with the void fraction of Spline interpolation. Finally, qualitative and quantitative results are presented and discussed.

1.3 Objectives

The main objective of this work is to improve void fraction measurement and image resolution from wire-mesh sensor with less than optimal electrodes number. This global objective is divided in eight parts, which are summarized by the Specific objectives:

1.3.1 Specific objectives

1. Review the related literature;
2. Estimate a sensitivity matrix by Finite Elements method (FEM);
3. Prepare the experimental setup in a horizontal two-phase liquid-gas flow loop;
4. Perform and record acquisition data simultaneously with 2 distinct WMS per experiment;
5. Design a Multivariate Gaussian flow model from experimental data;
6. Implement the image reconstruction method MAP with experimental data;
7. Validate and compare the proposed reconstruction method with spline interpolation;
8. Present further works.

1.4 Thesis outline

This work is organized as follows:

The Chapter 2 reviews the main theoretical concepts of multiphase flow that were important for the present thesis. In addition, we describe the wire-mesh sensor as well as its work principle. Finally, we present a brief review about image reconstruction methods.

The Chapter 3 details the procedure employed to model the sensitivity matrix by Finite Element Method (FEM). Then, the experimental setup is described. Finally, processing data tools are presented.

The Chapter 4 presents the results of the reconstruction method proposed. Here, MAP algorithm is compared with spline interpolation qualitatively and quantitatively.

Finally, in the Chapter 5 we summarizes the main contributions of this research as well as the further works.

Chapter 2

Background

This chapter presents a background of the indispensable concepts of multiphase flow as well as the math tools that were employed along of the thesis. Furthermore, it was introduced an image reconstruction method to improve WMS acquisition data.

2.1 Brief concepts of multiphase flow

Multiphase flow is defined as the simultaneous stream of two or more phases, which can occurs frequently in nature and industrial processes, e.g., the blood flowing in the human body or oil and gas transportation in pipelines and ducts (Falcone, Hewitt, & Alimonti, 2009). In the case of industrial systems, a wide effort has been made by researchers and industry to investigate and better understand this type of phenomena. This includes process optimization, models that describe the behavior of multiphase flow, development and improvement of flow metering, among others.

Although there are several types of multiphase flows, this work gives a special attention to the class of two-phase water-air flow, because these substances are easy to be experimentally manipulated and can be used as theoretical basis for more complex further works. In the following sections, we present the basic concepts of two-phase flows, e.g., pattern flows, derivate parameters and measurement instruments commonly used to measure multiphase flows.

2.1.1 Horizontal two-phase flow patterns

The phase interfaces of a two-phase flow into a system of a stream can assume different shapes and behaviors due to several factors. For example, velocity, fraction and properties of the phases; temperature and pressure of the flow; shape, diameter, inclination and roughness of the conduit, etc. These type of behaviors and shapes are known as “flow pattern” or “flow regime” (Falcone, Hewitt, & Alimonti, 2009). Some classifications of liquid-gas flow patterns streaming into a conduit is depicted in the Figure 2.1 and briefly explained as follows:

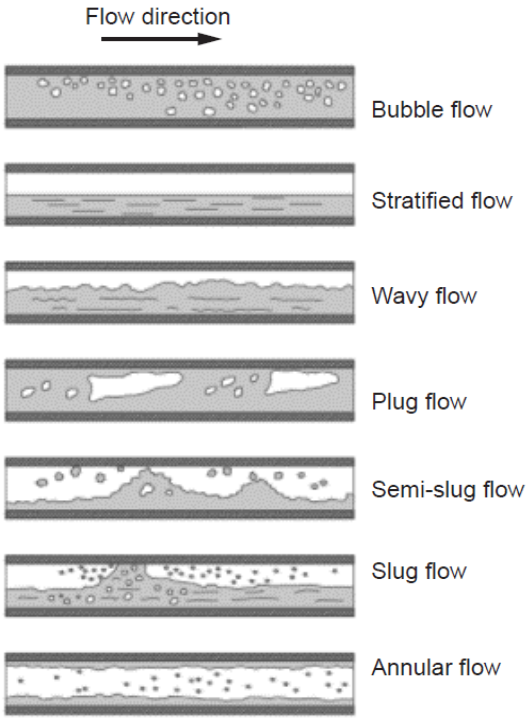

Figure 2.1: Horizontal two-phase flow patterns (Falcone, Hewitt, & Alimonti, 2009).

Bubble Flow: In this regime, dispersed bubbles move within the liquid phase. The bubbles are subject to coalesce with each other. They are characterized by non-regular form and by the complex movement within the flow.

Stratified Flow: Both phases are separated by the gravitational effects. In other words, the gas phase flows along the top part of the pipeline and the liquid phase flows along the bottom part.

Wavy Flow: This regime is similar to the stratified flow. However, due to the increase of the gas velocity, waves are formed on the liquid-gas interface.

Plug Flow: A sequence of bullet-shaped bubbles that flow along the top of the pipeline.

Slug Flow: The slug flow pattern occurs when the gas velocity is high enough to cause waves on the interface, which achieve the top of the tube filling totally the pipe cross-section. Bubbles dispersed may be observed in the liquid slug.

Annular Flow: In the annular flow regime, the liquid phase has a form of ring in the cross-section view. This occurs when the gas velocity is high enough to sustenance the liquid film at the wall of the conduit. In this way, the gas phase flows at the center of the pipe and the liquid phase at the borders.

Similarly, there are two-phase flow patterns for vertical or other intermediate angles of stream. Reader is referred to (Azzopardi, 2006) for details.

2.1.2 Two-phase flow pattern map

Transition between flow regimes has been investigated by many researchers. In this way, Taitel & Dukler (1976) developed a theoretical model to predict the transient of flow patterns in horizontal pipes. The model is based on physical concepts and no experimental data is needed. Since then, this method has been used widely to map the flow regime transitions in horizontal flows as shown in Figure 2.2.

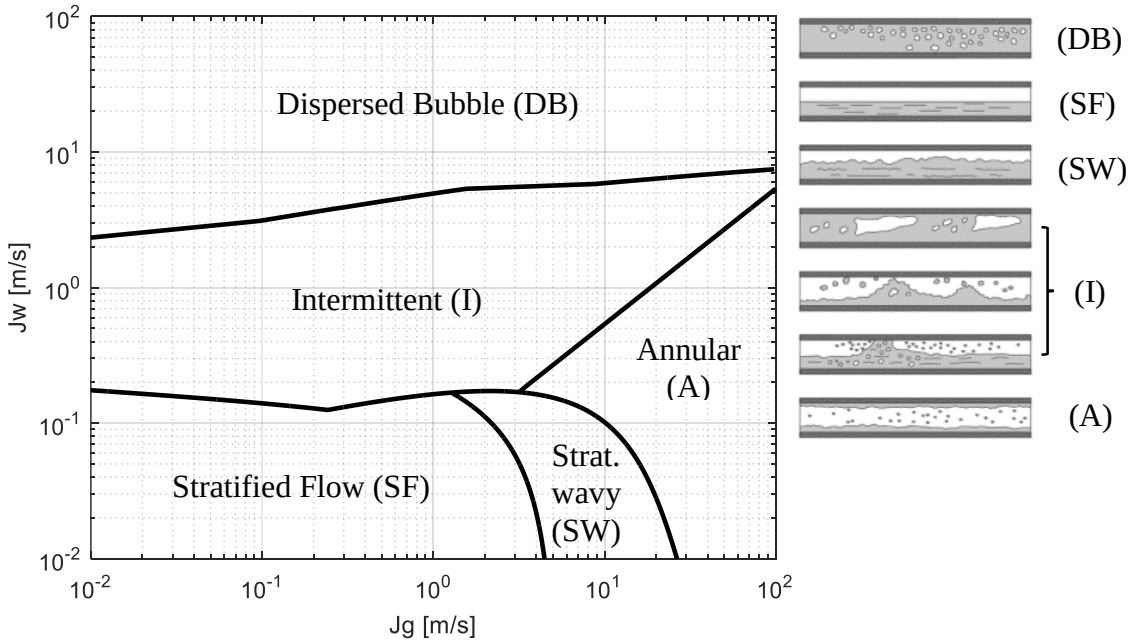

Figure 2.2: Horizontal two-phase flow pattern map (Taitel & Dukler, 1976).

The prediction of the flow regime is usually given by the relationship between the following parameters: Superficial velocity of the gas and water phases, duct diameter, and

properties of the fluids. However, through the flow pattern map depicts in Figure 2.2, only gas and water velocities (Jg and Jw) are needed. In the Chapter 3, the flow pattern map is used to indicate the operating points of experimental data employed in this work.

2.1.3 Two-phase flow parameter

a) Phase fraction

In this section, we introduce the concepts of phase fraction, which have been essential in several applications involving two-phase flow measurement. In particular, we give a focus on how to quantify and describe mathematically the phase fraction of gas-liquid flows. As definition, "void fraction" is the quantity of the gas phase and "hold-up" is the liquid phase. Both quantity are dimensionless and interchangeable, i.e., the sum of them is equal to 1.

According to Bertola (2003) and Da Silva (2008), before to define void fraction, it is essential to introduce the concept of phase indicator (or density) function, which provides binary information about the presence or absence of the phase k at a spatial position $\mathbf{x}$ at the time t. This function is described as

$$P_k(\mathbf{x},t)=\begin{cases}1 & \text{if } \mathbf{x}\in D_k\\ 0 & \text{if } \mathbf{x}\notin D_k\end{cases}, \tag{2.1}$$

where D is a three dimensional geometrical domain and the index k is used in the case of this work to refer to the gas or liquid phase $(k=G,\ L)$, that is, D_G and D_L are subsets of the domain D. In this way, the first definition of void fraction is given by averaging the gas indicator function (2.1) over the time. It is known as *Local void fraction* and defined as

$$\alpha(\mathbf{x})=\lim_{T\to\infty}\frac{1}{T}\int_T P_G(\mathbf{x},t)dt. \tag{2.2}$$

When the time T tends to infinity, the Equation (2.2) results in

$$\alpha(\mathbf{x})=\frac{T_G}{T}=\frac{T_G}{T_G+T_L}, \tag{2.3}$$

where, T_G and T_L are the cumulated time that the gas and the liquid phase occupied a spatial point $\mathbf{x}$ given time T. The definition of local void fraction can be expanded for one or more dimensions. In this way, the two-dimensional void fraction (also known as cross-sectional

average void fraction) is given from averaging the indicator function (2.1) over the area A at a given time:

$$\alpha_{cs}(t) = \frac{1}{A}\int_A P_G(\mathbf{x},t)da = \frac{A_G}{A}, \tag{2.4}$$

Here, the Equation (2.4) is given by the ratio between the cumulated area occupied by the gas phase and the total of the cross-sectional area at time t. This formulation is useful in many measurement systems, e.g., instruments operated by means of radiation attenuation or electrical impedance techniques.

b) Superficial velocity

Other indispensable parameter in the context of multiphase flow is the superficial velocity of phases. As seen in the section 2.1.2, the superficial velocity of liquid and gas can be used to indicate the flow pattern through a flow pattern map. In this way, the phase velocity *j* is calculated by

$$j_k = \frac{Q_k[m^3/s]}{A_k[\mathrm{m}^2]}, \tag{2.5}$$

where, *Q* and *A* are the volumetric flow rate and pipe cross-sectional area, respectively, given a phase *k.* Thus, the total velocity of water-gas mixture streaming inside the pipe is

$$j_T = j_W + j_G, \tag{2.6}$$

here, the indexes *W* and *G* represent the water and gas phases, respectively.

In the next section, we focus on the Wire-Mesh sensor. Its principle work is based on impedance techniques and is used to measure local phase fraction of multiphase flow.

2.2 Wire-mesh sensor concepts

Wire-mesh sensor (WMS) is a device that has been used for the high temporal visualization of two-phase flow. The first generation of WMS was proposed by Prasser et al. (1998). It is composed by two electrode planes axially spaced by a millimeter distance d_z perpendicular to the flow direction (Figure 2.3(b)). The planes of electrode wires cross under an angle of 90° and are used as transmitters and receivers, respectively (Figure 2.3(a)). Both planes contain a number of parallel thin stainless steel wires stretched over the pipe cross section.

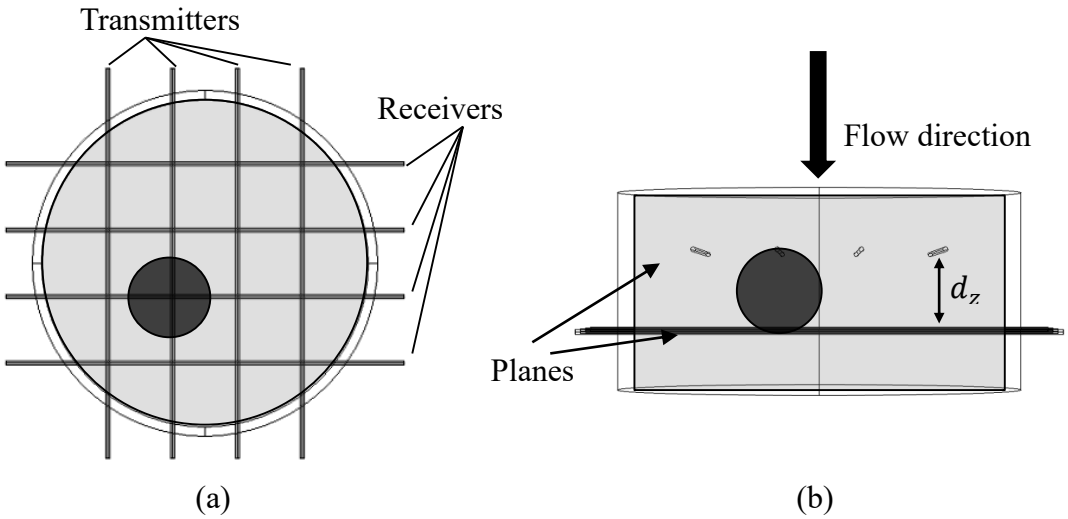

Figure 2.3: Scheme of Wire-Mesh Sensor: (a) transmitters and receivers cross under an angle of 90°; (b) two planes axially spaced by a small distance perpendicular to the flow direction.

Each crossing point between transmitter and receiver wires measures an electrical signal proportional to the local instantaneous void fraction of the two-phase flow. Actually, three types of measurement are available:

Conductivity measurement: it is used to measure two-phase flows, where one phase is conductive and the other is non-conductive, i.e. water and gas. It works applying a bi-polar pulse that excite the first transmitter wire, while all other wires are put on zero differential (Figure 2.4 (a)). Thus, an analog current is measured, which is function of the conductivity of the mixture located in the gap between the transmitter and receptor wires. Consequently, when the gap is occupied by a conductive phase volume, the receptor measures a higher current than a non-conductive phase. The signal measured is then converted to voltage and stored as a digital signal. This procedure is repeated for all transmitter wires through a multiplex circuit. In the end of the measuring cycle, a two-dimensional matrix of values of voltage is generated. Finally, the raw data of the matrix can be processed and converted to the instantaneous void fraction of the pipe cross section.

Permittivity measurement (capacitive): proposed by Da Silva (2008), it is also used to measure two-phase flows. However, using capacitive properties, it is possible evaluate the instantaneous void fraction of some non-conductive phase mixtures, i.e. oil-gas. The procedure is the same of the previous method (conductivity), but the bi-polar signal is substituted by a sinusoidal wave with a constant frequency (Figure 2.4 (c)). Both phases can be distinguished by the linear relationship between current measured and capacitance (permittivity) of each

phase. In this approach, it is assumed that each crossing-point of the sensor behaves as a capacitor, individually, where transmitter and receptor wires are two parallel conductors and the gap between the crossing point wires is the dielectric environment.

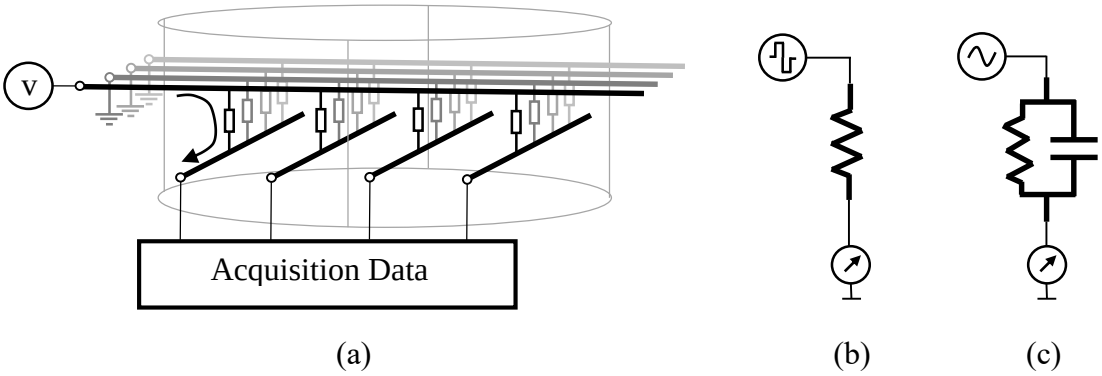

Figure 2.4: Electrical properties of measurement of the crossing-points: (a) lateral view of the WMS, where the gap of each crossing-point represents a single impedance; (b) The impedance is purely resistive in the conductivity principle; (c) The impedance behaves as a capacitor due to the high excitation frequency.

Dual-modality: Based on both measuring principles, Dos Santos, et al. (2015) proposed a dual-modality for wire-mesh sensor in order to allow three-phase flow visualization. The method consists on simultaneous excitation with two distinct frequencies, which have relationship between conductive and capacitive parts of the flow impedance.

2.2.1 Wire-mesh for visualization of two-phase flow

As described previously, the WMS crossing-points measure the local instantaneous void fraction of the pipe cross-section. When a measuring cycle is concluded, the resulting matrix can be used for visualization of the cross-sectional distribution of the phases over pipe cross section. Figure 2.5 (a) shows a standard 16x16 WMS developed at the Helmholtz-*Zentrum* Dresden-Rossendorf (HZDR) and Figure 2.5 (b) illustrates a commercial software for visualization of WMS data.

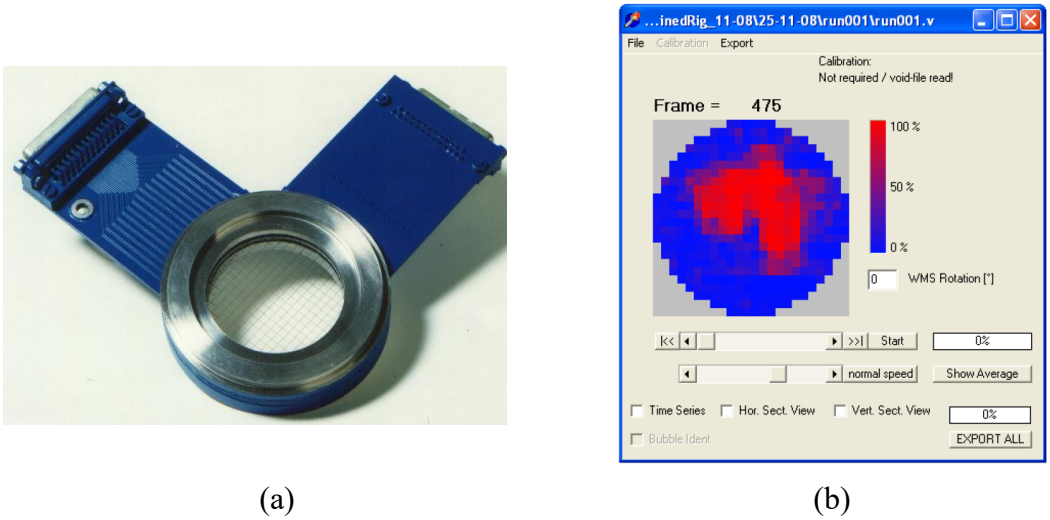

(a) (b)

Figure 2.5: Wire-mesh sensor. (a) 16x16 Standard Sensor (b) Visualization of cross-sectional image of a 24x24 WMS (Thiele & Hampel, 2010).

In the classical operating mode, no reconstruction method is needed and the value measured by a single crossing-point is approximated as a square pixel with size of d_w mm (Figure 2.6). Consequently, the resolution of the sensor is equal to the number of crossing-points and depends on the spacing between the electrode wires. The accuracy of this approach was investigated by Nuryadin, et all. (2015). In their work, an experimental study was carried out to evaluate the dependence of bubble size in a two-phase liquid-gas flow. In addition, they found deviation less than 10% to measure and estimate volume of bubbles using WMS.

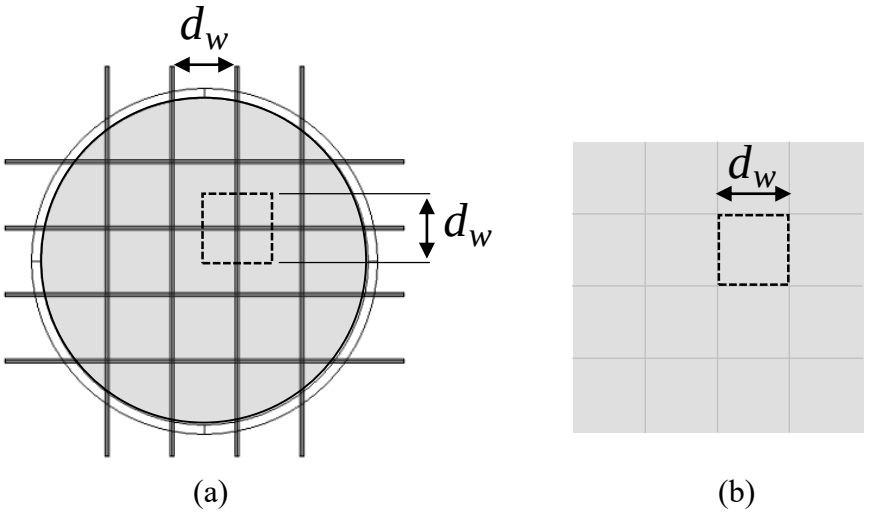

(a) (b)

Figure 2.6: Image of Wire-mesh sensor by the classical approach. (a) Relationship between the spacing of wires and pixel; (b) Array of pixels of a WMS.

2.2.2 Simulation

A more detailed description of the physical behavior within the crossing point of the capacitive WMS is given by Da Silva (2008) and Wagner (2008). They have considered the system as an electrostatic problem, since the sensor dimensions are much smaller than the wavelength of electrical fields employed. Figure 2.7 depicts the voltage distribution of a simplified 5x5 WMS model used by Da Silva (2008). Here, a single electrode wire was excited and the other wires were put on zero differential. Based on this principle, sensitivity distribution of the sensor can be modelled and incorporated in image reconstruction algorithms (more details in section 3.2).

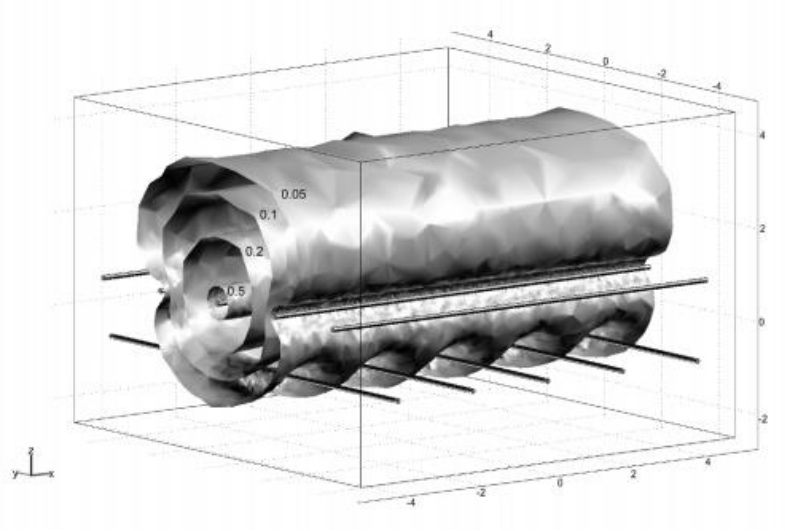

Figure 2.7: Voltage distribution of a single transmitter wire simulated by FEM. Values of each isosurface are given in volts (Da Silva, 2008).

The electrostatic problem depicted in Figure 2.7 is solved by Finite Element Method (FEM). In the simulation stage, a voltage V excites the transmitter wire, which is calculated by the Poisson's equation

$$\nabla(\varepsilon_0 \varepsilon(\mathbf{r}) \nabla V(\mathbf{r})) = 0, \tag{2.7}$$

where $\mathbf{r}$ is the position vector, ε_0 is the permittivity of vacuum and ε is the relative permittivity of the environment. The free charge density ρ in the material is assumed equal to zero. The domain has a form of a cube and all lateral faces satisfying the relationship $\mathbf{n}.\mathbf{D} = 0$. In other words, the normal component of the electric displacement equals zero. The transmitter wire excited is set to +1 V while the all other are on ground potential.

The capacitance analyses is carried out as post-processing and calculated by the surface integral of the receiver wire in the form

$$C_{\text{sim}} = \frac{1}{V}\int_{\Gamma} \rho(\Gamma)\cdot d\Gamma, \tag{2.8}$$

here, ρ is the charge density and Γ are the receiver wire boundaries. According to Equations (2.7)- (2.8), Da Silva (2008) proposed an approximation for the spatial sensitivity of the WMS given by:

$$\psi = \frac{\Delta C}{\max(\Delta C)}, \tag{2.9}$$

where ΔC is the difference between the capacitance undisturbed and disturbed. Based on this principle, some researches have modified Equation (2.9) and used it as a sensitivity map to improve resolution of WMS data (Sun & Wang, 2011) and (Weimin, Li, & Peng, 2016). In both studies, the sensitivity map is used as *a Priori* information to solve inverse problems. Here, Sun (2011) and Weimin (2016) proposed methods based on inverse problems to increase resolution of WMS data with optimal electrode wires. On the other hand, our method has been destined in the cases of WMS with less than optimal electrode wires (Dias, Pipa, & Da Silva, 2016).

2.3 Increasing image resolution

The Wire-mesh sensor was developed with the goal of avoiding the use of tomographic reconstruction algorithms (Prasser, 1998). Therefore, the direct acquisition of the sensor is robust and saves computational processing. However, the image resolution is limited by the number of crossing points of transmitter and receiver wires. Since many processes require higher image resolution, two alternatives may be used to improve resolution of WMs data: (1) Increasing the number of electrode wires; (2) Using signal processing techniques based on *inverse problem*. The first option is simpler and keeps stability and robustness during the acquisition. However, by increasing the number of electrode wires, the intrusive effects in the flow are increased drastically. This option is usually discarded because the intrusive effects can be undesired in many processes. Therefore, this work proposes an alternative based on the second option. This alternative will be used to increase resolution of wire-mesh sensor data with less than optimal electrode wires. In this way, the intrusive effects is reduced and the image

resolution improved, simultaneously. Before detailing the reconstruction method used in this work, we discuss the following concepts:

a) Spline interpolation

Interpolation techniques can be used to increase size of images. A particular case of interpolation is the spline method. According to Unser (1999), splines are piecewise polynomials with pieces smoothly connected. In the case of WMS, the joint points of the polynomials (*knots*) are the observed data. The B-spline expansion is described in the form

$$s(x) = \sum_{k \in Z} c(k)\beta^n(x-k), \tag{2.10}$$

where, $c(k)$ is the B-spline coefficients (observed data **f** from WMS), and $\beta^n(x)$ is a function shifted by k and degree n called central B-spline. Figure 2.8 presents the B-splines of degrees from 0 to 3.

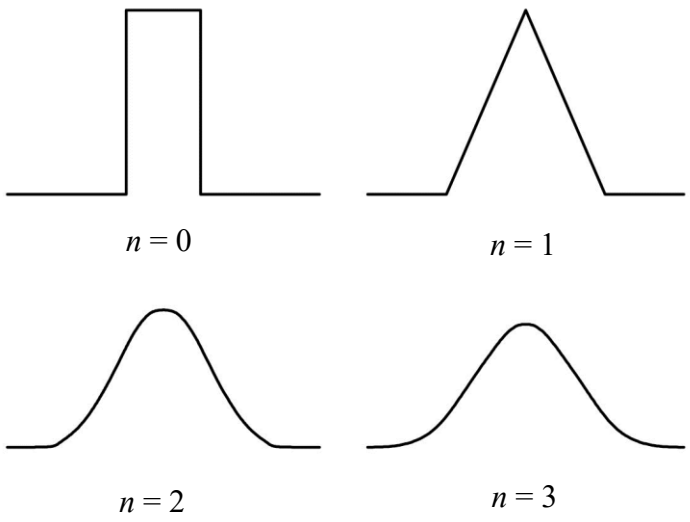

Figure 2.8: Central B-spline of degree from 0 to 3 (Unser, 1999).

The B-spline of degree 3 is known as cubic spline. This particular case of spline tends to be the most popular in application (Unser, 1999). It is also often employed for performing high-quality interpolation. Figure 2.9 exemplifies a cubic spline of a set of observed data.

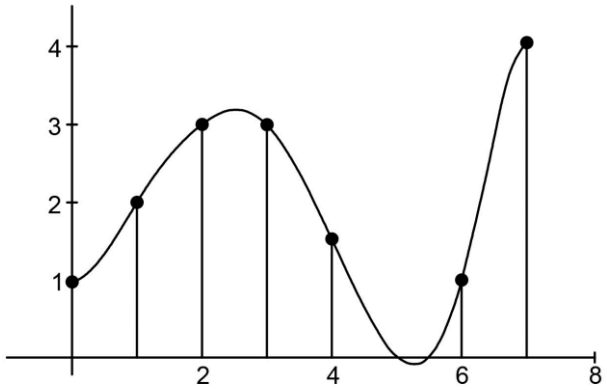

Figure 2.9: Example of a cubic spline signal (Unser, 1999).

Since spline interpolation works as a low-pass filter, the quality of the reconstruction from an aliased low-resolution (LR) image is limited. In other words, it cannot recover high frequency components degraded or lost during the acquisition. For this reason, it is necessary to use alternative methods able to recover such frequencies.

b) Super-resolution image reconstruction

As explained by Park (2003), Super-resolution techniques is the fusion of information from several observations of the same scene. That is, multiple low-resolution (LR) images provide the new information necessary to obtain the high-resolution (HR) image. In this way, the LR images must be shifted with subpixel precision as illustrated in Figure 2.10.

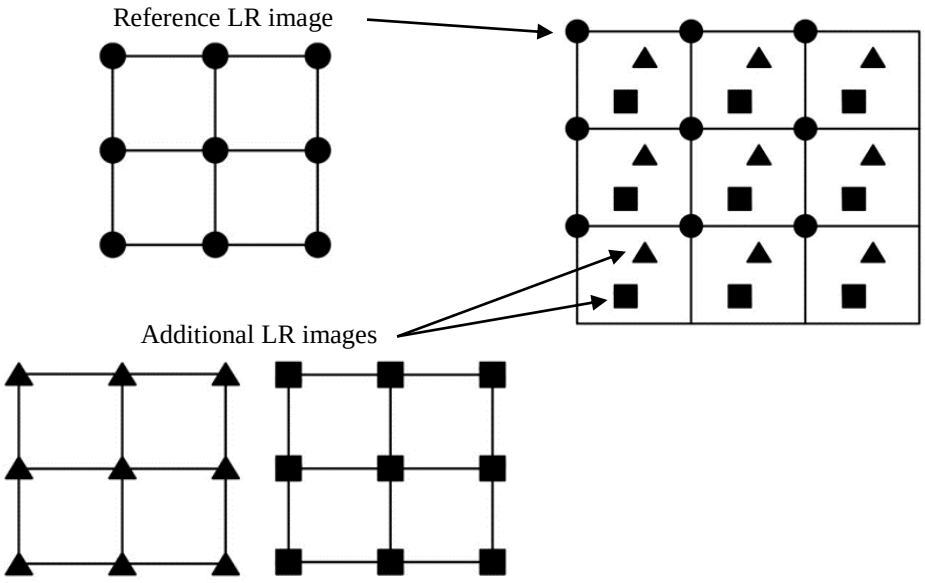

Figure 2.10: Basic premise for super resolution: If there exist subpixel shifts between LR images, then super resolution reconstruction is possible (Park, 2003).

The LR images can be obtained from multiple observations located in different positions or by several scenes from a single point. Different from (Park, 2003), we used experimental WMS flow data with HR to determine a Multivariate Gaussian flow model (MGFM), which is the new information needed to solve the SR problem. In this way, it was employed a 16x16 WMS with electrode wires shifted with subpixel precision when compared with LR WMS with less than optimal number of electrode wires. Thus, statistical parameters were extract from experimental flow data of the 16x16 WMS and used to increase resolution of the LR WMS by Maximum *a posteriori* (MAP) algorithm. Before introducing such algorithm, we will present the model of LR image acquisition of WMS in the following subsection.

2.3.1 Linear model approach

In order to increase resolution of a WMS, the acquisition model of a low-resolution (LR) sensor is described as a linear problem in the form

$$\mathbf{g} = \mathbf{W}\mathbf{f} + \mathbf{v}, \tag{2.11}$$

where, $\mathbf{g} \in \mathbb{R}^{N\times 1}$ is a vector of data acquisition of WMS with less electrode wires then optimal. The operator $\mathbf{W} \in \mathbb{R}^{N\times M}$ is the sensitivity map and can be rewritten as the product of two operator: **H** and **S**. Here, **H** describes the influence of a pixel of a high-resolution image of WMS in the acquisition data (point-spread function (PSF)) and the matrix **S** is a subsampling operator, which is able to decrease resolution of WMS sensor data. $\mathbf{f} \in \mathbb{R}^{M\times 1}$ is a vector that represents the cross-sectional image of the pipe with the optimal resolution and $\mathbf{v} \in \mathbb{R}^{N\times 1}$ is measurement noise. It is necessary to notice that both images $\mathbf{g}$ and $\mathbf{f}$ are represented in a lexicographical order. In other words, the two-dimensional matrix used for visualization of the two-phase flow is ordered as a vector as follows:

$$\begin{bmatrix} g_1 \\ g_2 \\ \vdots \\ g_N \end{bmatrix} = \begin{bmatrix} \mathbf{w}_1^{\mathrm{T}} \\ \mathbf{w}_2^{\mathrm{T}} \\ \vdots \\ \mathbf{w}_N^{\mathrm{T}} \end{bmatrix} \begin{bmatrix} f_1 \\ f_2 \\ \vdots \\ f_M \end{bmatrix} + \begin{bmatrix} v_1 \\ v_2 \\ \vdots \\ v_N \end{bmatrix}. \tag{2.12}$$

The Equation (2.11) or (2.12) are so-called *direct problem.* Once known the operator $\mathbf{W}$, to find the observation data from the high-resolution image is usually a trivial task. However, in practice, we are interested to find $\hat{\mathbf{f}}$, which represents the estimate of $\mathbf{f}$ given the observation data $\mathbf{g}$. A basic solution for this problem is given by back projection method:

$$\hat{\mathbf{f}} = \mathbf{W}^{\mathrm{T}}\mathbf{g}. \tag{2.13}$$

This type of operation is known as *inverse problem*, and may be hardly solved, because in the case of the WMS, the operator **W** has insufficient information to increase data resolution. Thus, it is indispensable the employment of *a Priori* knowledge and regularization to achieve feasible results.

2.3.2 Maximum a posteriori

With the purpose to solve the problem of indeterminacy and provide feasible images when the WMS data is reconstructed, we used a statistical view of regularization (Kay, 1993), (Bovik, 2000). The goal of this method is to find the maximum *a posteriori* (MAP) estimate of the unknown image $\mathbf{f}$ as that maximizes the posterior density $p(\mathbf{f}\,|\,\mathbf{g})$ in the form

$$\hat{\mathbf{f}}_{\mathrm{MAP}} = \arg\max_{\mathbf{f}} p(\mathbf{f}\,|\,\mathbf{g}). \tag{2.14}$$

Applying the Bayes rule, we obtain

$$p(\mathbf{f}\,|\,\mathbf{g}) = \frac{p(\mathbf{g}\,|\,\mathbf{f})\,p(\mathbf{f})}{p(\mathbf{g})}, \tag{2.15}$$

once $p(\mathbf{g})$ is constant and using logarithm properties, this problem can be solved as a minimization

$$\hat{\mathbf{f}}_{\mathrm{MAP}} = \arg\min_{\mathbf{f}} \{-\log p(\mathbf{g}\,|\,\mathbf{f}) - \log p(\mathbf{f})\}, \tag{2.16}$$

where $\log p(\mathbf{g}\,|\,\mathbf{f})$ is the log-likelihood function and $\log p(\mathbf{f})$ is a term dependent only on $\mathbf{f}$, called the prior model, which allows incorporate priori knowledge about $\mathbf{f}$ into the estimate.

Assuming that the likelihood function and the Prior term are Gaussian Probability Function Density (PFD), both are described in the form:

$$p(\mathbf{g}\,|\,\mathbf{f}) = \frac{1}{\sigma_{\nu}\sqrt{2\pi}} \exp\left\{-\frac{\|\mathbf{g}-\mathbf{W}\mathbf{f}\|^2}{2\sigma_{\nu}^2}\right\}, \tag{2.17}$$

and,

$$p(\mathbf{f}) = \frac{1}{|\Sigma_{\mathbf{f}}|^{1/2}\sqrt{2\pi}} \exp\left\{-\frac{1}{2}(\mathbf{f}-\boldsymbol{\mu}_{\mathbf{f}})^{\mathrm{T}}\Sigma_{\mathbf{f}}^{-1}(\mathbf{f}-\boldsymbol{\mu}_{\mathbf{f}})\right\}. \tag{2.18}$$

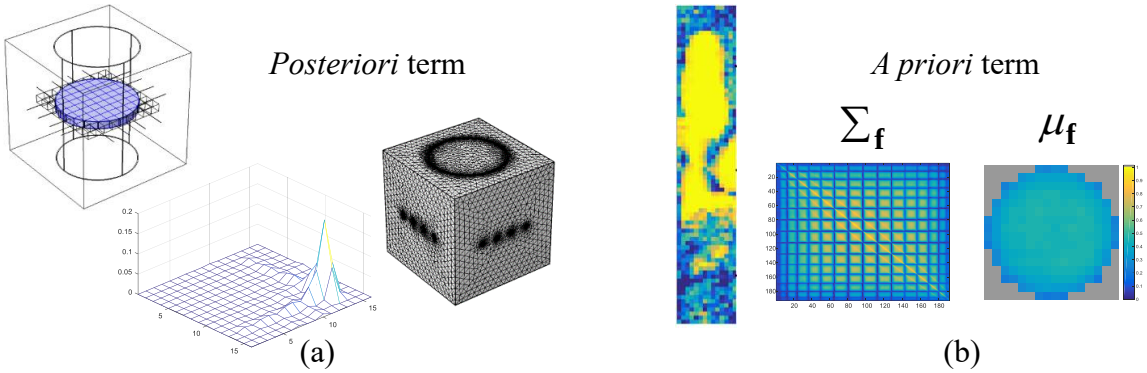

Figure 2.11: Parameters to solve MAP. (a) Sensitivity operator by FEM; (b) Statistical parameters of the flow.

Substituting the Equations (2.17) and (2.18) on the Equation (2.16), the MAP can be solved by

$$\hat{\mathbf{f}}_{\text{MAP}} = \frac{\partial}{\partial \mathbf{f}} \left\{ c - \exp\left\{ -\frac{\|\mathbf{g} - \mathbf{W}\mathbf{f}\|^2}{2\sigma_\nu^2} \right\} + c - \exp\left\{ -\frac{1}{2}(\mathbf{f} - \boldsymbol{\mu}_{\mathbf{f}})^{\mathrm{T}} \boldsymbol{\Sigma}_{\mathbf{f}}^{-1} (\mathbf{f} - \boldsymbol{\mu}_{\mathbf{f}}) \right\} \right\} = 0, \qquad (2.19)$$

which has analytical solution as follows:

$$\hat{\mathbf{f}}_{\text{MAP}} = (\mathbf{W}^{\mathbf{T}}\mathbf{W} + \sigma_\nu^2 \boldsymbol{\Sigma}_{\mathbf{f}}^{-1})^{-1} (\mathbf{W}^{\mathbf{T}}\mathbf{g} + \sigma_\nu^2 \boldsymbol{\Sigma}_{\mathbf{f}}^{-1} \boldsymbol{\mu}_{\mathbf{f}}). \qquad (2.20)$$

Here, the regularization by the Multivariable Gaussian Model (MGM) (2.20) can be used to increase resolution of WMS LR data. The sensitivity map $\mathbf{W}$ is solved by Finite Element Method (FEM) (Figure 2.11(a)) (see section 3.2). The statistical parameters $\boldsymbol{\Sigma}_{\mathbf{f}}$ and $\boldsymbol{\mu}_{\mathbf{f}}$ are estimated by experimental flow data from a 16x16 WMS (Figure 2.11(b)). Finally, σ_ν^2 is the variance of the measuring noise, which is frequently substituted by a regularization factor λ. In this way, due to the difficult to estimate the measuring noise in a practical context, λ can be empirically tuned. Rearranging the Equation (2.20) and making $\sigma_\nu^2 = \lambda$, the minimization problem can be described in the form:

$$\hat{\mathbf{f}}_{\text{MAP}} = \boldsymbol{\mu}_{\mathbf{f}} + \boldsymbol{\Sigma}_{\mathbf{f}} \mathbf{W}^T (\mathbf{W}\boldsymbol{\Sigma}_{\mathbf{f}} \mathbf{W}^T + \lambda \mathbf{I})^{-1} (\mathbf{g} - \mathbf{W}\boldsymbol{\mu}_{\mathbf{f}}). \qquad (2.21)$$

Both equations (2.20) and (2.21) are equivalents. However, in the case of WMS, Equation (2.21) is more appropriate because the sensitivity map $\mathbf{W}$ need not be full rank to ensure the invertibility of $\mathbf{W}\boldsymbol{\Sigma}_{\mathbf{f}}\mathbf{W}^T + \lambda\mathbf{I}$.

Other classes of reconstruction image may be used to recover HR WMS data from observed LR image. Future work should compare more methods in order to identify advantages and limitations of each one. In the next chapters, we give more information about MGM in a

practical context as well as details to estimate the sensitivity map by FEM. In Chapter 4, MAP algorithm is compared with spline interpolation and the results are discussed.

Chapter 3
Increasing resolution of wire-mesh sensor data

In this chapter, we detail the methodology adopted to increase resolution of wire-mesh sensor data with less electrode wires than optimal.

3.1 Introduction

As mentioned previously, the goal of this work is to improve resolution of Wire-Mesh sensor data with less than optimal electrode wires. Since conventional reconstruction methods give poor solutions (back projection and minimum-norm), we propose a reconstruction method based on Multivariable Gaussian Flow Model (MGFM). In this case, statistical parameters from experimental flow data are used as regularization. For a better understanding, the Figure 3.1 summarizes the topics adopted to implement and evaluate the proposed reconstruction, which will be divided in two parts (solid and dashed boxes). In this chapter, we introduce the contents of solid boxes. Here, main aspects of the methodology are presented, i.e. modeling a sensitivity map from FEM (part of the WMS acquisition model); the use of a horizontal flow loop to perform experiments in order to estimate statistical parameters employed as regularization of inverse problem. In the dashed boxes (Chapter 4), we detail and discuss experimental and numerical results of the reconstruction method proposed.

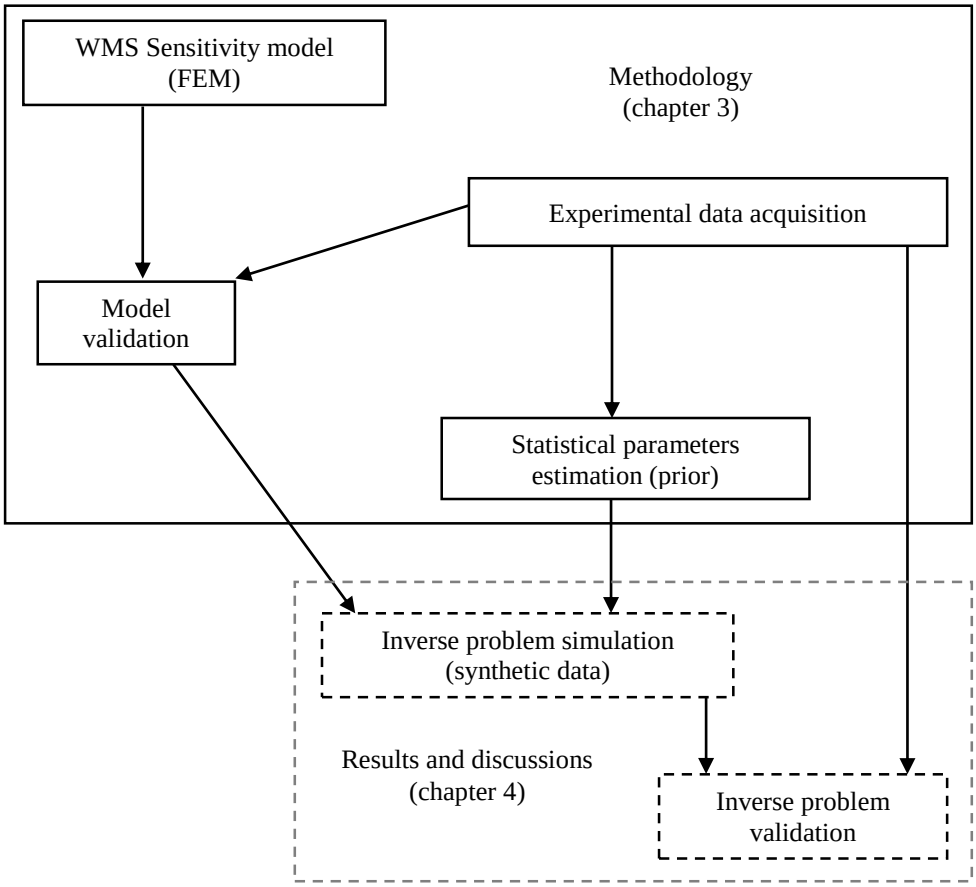

Figure 3.1: Topics that describe the methodology of the present research.

3.2 Numerical simulation

A Wire-Mesh sensor is built with simple mechanical architecture. However, its physical behavior is hard to be described mathematically due to nonlinearities and the round geometry. An easier way is to estimate the electrical field of the sensor using Finite Element Method (FEM). For this purpose, we used the commercial software COMSOL Multiphysics 5.0. This program estimate efficiently electrostatic problems by solving Partial Differential Equations (PDE). In the following steps, we describe the model components as well as the strategies adopted to calculate the acquisition sensitivity, which will be approximated by a model to increase resolution of WMS data.

3.2.1 Model components

The main components of the sensor were represented in the software Comsol as illustrated in the Figure 3.2. The sensitivity area was divided in 256 parts with shape of rectangular cuboids, which are the same number and position of crossing points of an optimal 16x16 WMS. In this

way, however, due to the round format of the pipe, some borders of the sensitivity area located out of the pipe were disregarded during the simulation. In other words, from 256 divisions, solely 208 have been used as perturbation. The center of the upper face of each cuboid matches with the crossing points of an imaginary 16x16 WMS. For a better representation, electrical permittivity of some materials were incorporated to the model. That is, acrylic (pipe), steel (wires), water (volume inside the pipe and sensitivity area) and air (universe, divisions out the pipe and perturbation).

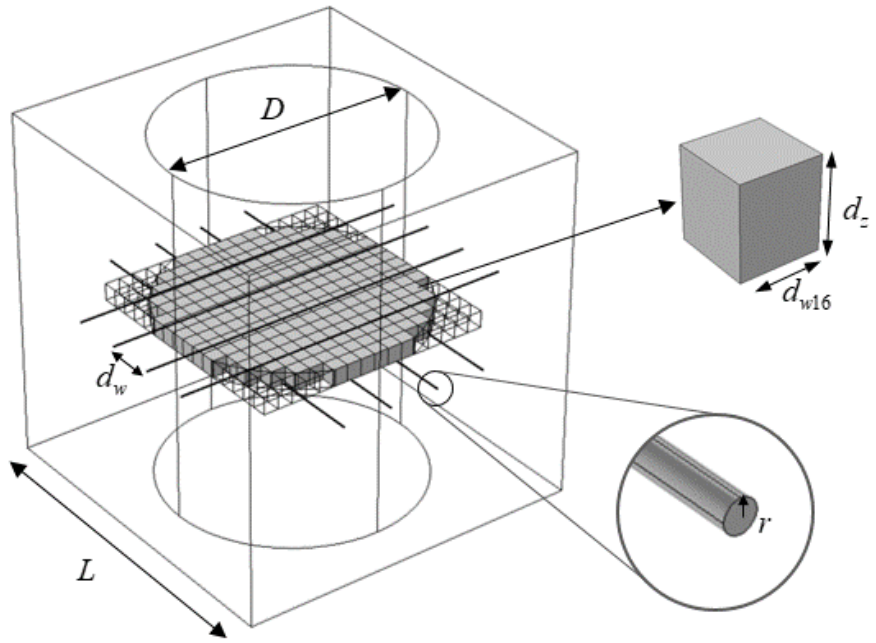

Figure 3.2: Components of a 4x4 WMS model designed in the software Comsol.

Size of the components of the model are summarized in the Table 3.1. Note that the spacing between electrode wires is given by $D/(N+1)$, where N is the number of transmitter wires. Thus, a single model was created for each case: 8x8, 6x6, 4x4 and 2x2.

Table 3.1: Parameters used to design the components of a WMS by the software Comsol.

L	D	r	d_{w16}	d_w	d_z
50 mm	25.4 mm	0.06 mm	1.59 mm	$D/(N+1)$	1.8 mm

After designing a wire-mesh model, we tried to find the best mesh with the goal to balancing simulation time and numerical error. In the context of the WMS, however, mesh refinement procedure is not trivial to be performed due to the huge difference in scale between

the small and the large components, that is, diameter of wires and universe, respectively. Thus, we decided to use recommended settings by the software Comsol to avoid errors during the mesh generation procedure.

Although no detailed study about mesh optimization has been done, it supposed that mesh models presented in this work are comparable, because the residual error occurs with similar condition for each one. The Figure 3.3 exemplary depicts the mesh built with default configuration of a 4x4 WMS.

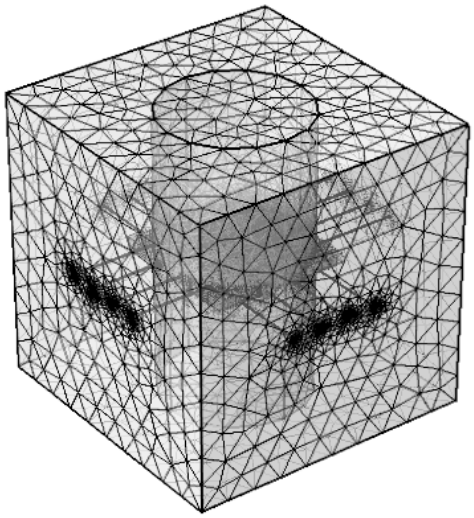

Figure 3.3: Mesh of a 4x4 WMS created by the software Comsol.

In further works, convergence mesh study should be investigated. (See (Libert, 2013)).

3.2.2 Sensitivity map of WMS

The sensitivity map is estimated by placing a perturbation within the sensitivity area of the Wire-mesh (space between the two wire planes) and measuring the effects of this perturbation in a given crossing-point capacitance. In this way, the capacitance of the crossing-points were calculated by solving the following surface integral of the receptor electrode

$$C(i,j) = \frac{1}{V}\int_{\Gamma} \rho(\Gamma)\cdot d\Gamma, \tag{3.1}$$

The indexes *j* and *i* represents the crossing-point analyzed and the position of the perturbation, respectively. The sequence of the perturbation is showed in the Figure 3.5, where solely one perturbation is applied per time. The constant V is the voltage applied in the transmitter electrode and ρ is the charge density over the wire boundaries Γ.

Based on the Equation (3.1), the procedure used in this work to estimate the sensitivity map is composed by *N* steps (Figure 3.4). Where *N* is the number of crossing-points of the WMS.

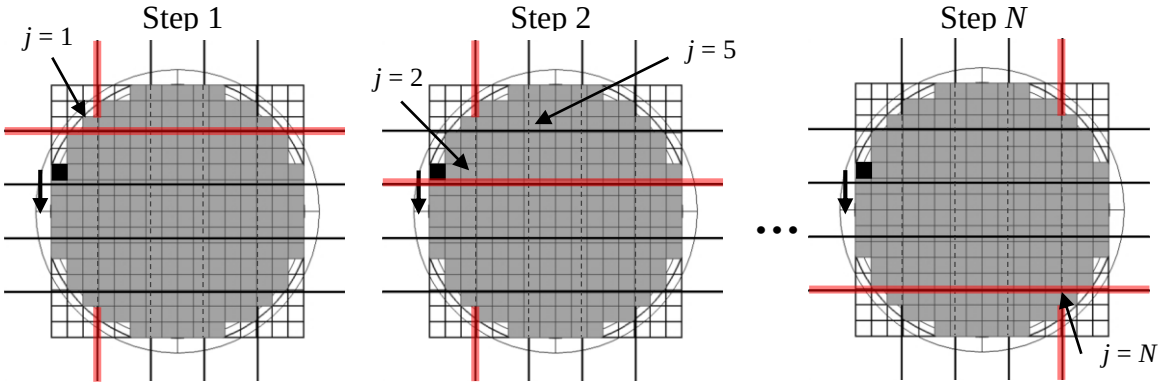

Figure 3.4: Steps to estimate a sensitivity map of a 4x4 WMS, where the red lines represents the crossing point activated.

In the first step, the perturbation is placed in the position 1 and the capacitance of the crossing-point with index $j = 1$ is calculated by the Equation (3.1). Thus, the perturbation sweeps along the sensitivity area according with the sequence showed in the Figure 3.5. In this way, 208 values of capacitance referent to the crossing point 1 is estimated. During a given measurement, the perturbation changes electric permittivity of its position to 1 (relative permittivity of air), while the other divisions into the sensitivity area stay with relative permittivity of the water (80). Table 3.2 summarizes the electrical permittivity of all materials of the model.

					57	73	89	105	121	137				
			29	43	58	74	90	106	122	138	153	167		
		17	30	44	59	75	91	107	123	139	154	168	181	
	7	18	31	45	60	76	92	108	124	140	155	169	182	193
	8	19	32	46	61	77	93	109	125	141	156	170	183	194
1	9	20	33	47	62	78	94	110	126	142	157	171	184	195	203
2	10	21	34	48	63	79	95	111	127	143	158	172	185	196	204
3	11	22	35	49	64	80	96	112	128	144	159	173	186	197	205
4	12	23	36	50	65	81	97	113	129	145	160	174	187	198	206
5	13	24	37	51	66	82	98	114	130	146	161	175	188	199	207
6	14	25	38	52	67	83	99	115	131	147	162	176	189	200	208
	15	26	39	53	68	84	100	116	132	148	163	177	190	201	
	16	27	40	54	69	85	101	117	133	149	164	178	191	202	
		28	41	55	70	86	102	118	134	150	165	179	192		
			42	56	71	87	103	119	135	151	166	180			
					72	88	104	120	136	152				

Figure 3.5: Index of the sensitivity area (positions between 1 and 208) and the borders (gray blocks).

Table 3.2: Material and electrical permittivity parameter of the components of the WMS model.

		Electrical permittivity ε		
Components	Material	Measurement	High calibration	Low calibration
Universe and transparent boxes	Air	1	1	1
Pipe	Acrylic	1	1	1
Inside the pipe	Water/air	80	80	1
Wires	Steel	1	1	1
Sensitivity area (grey boxes)	Water/air	80 or 1	80	1
Perturbation (black box)	Air	1	80	1

Once the Step 1 is concluded, this procedure is repeated N times (total number of crossing points). Thus, the 208 values of capacitance solved from the Step 1 are part of the first line of the capacitive distribution matrix, as follows:

$$\mathbf{C} = \begin{bmatrix} C(1,1) & \cdots & \cdots & \cdots & C(1,208) \\ & \ddots & & & \\ \vdots & & \ddots & & \vdots \\ C(N,1) & \cdots & \cdots & \ddots & \mathrm{C}(N,208) \end{bmatrix}. \tag{3.2}$$

In practice, the sensitivity matrix must be normalized by the relationship

$$w(i,j) = \frac{C_{\mathrm{H}}(j) - C(i,j)}{C_{\mathrm{H}}(j) - C_{\mathrm{L}}(j)}, \tag{3.3}$$

where, C_{H} and C_{L} are capacitance calculated by Equation (3.1) with the pipe full of water and full of gas, respectively. In addition, each variable C is a simulated capacitance when a single perturbation is applied into the sensitivity area. Employing calibration function (3.3) in the matrix (3.2), we find

$$\mathbf{W} = \begin{bmatrix} w(1,1) & \cdots & w(1,M) \\ & \ddots & \\ \vdots & \ddots & \vdots \\ w(\mathrm{N},1) & \cdots & w(\mathrm{N},\mathrm{M}) \end{bmatrix}. \tag{3.4}$$

Here, the sensitivity matrix **W** is simultaneously a linear combination between point-spread and subsampling functions that is given by:

$$\mathbf{W} = \mathbf{HS}, \tag{3.5}$$

thus, the matrix **H** describes the influence of a pixel of a high-resolution image of WMS in the acquisition data (point-spread function (PSF)). The matrix **S** is a subsampling operator, which is able to decrease resolution of WMS sensor data. Thus, the acquisition of wire-mesh sensor can be approximated by a linear model in the form

$$\mathbf{g} = \mathbf{Wf}. \tag{3.6}$$

In this way, the operation to find the acquisition vector **g** given a high-resolution frame of WMS **f** is usually trivial (Figure 3.6).

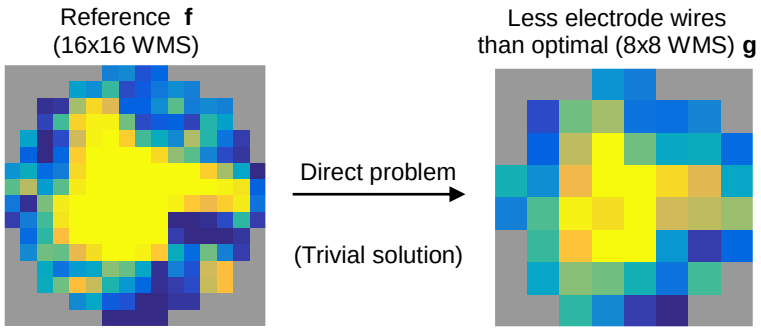

Figure 3.6: Example for direct problem.

On the other hand, the estimate of $\hat{\mathbf{f}}$ may be a challenge. For example, by employing *linear back projection* (LBP):

$$\hat{\mathbf{f}} = \mathbf{W}^{\mathbf{T}}\mathbf{g}, \tag{3.7}$$

or, by minimum-norm:

$$\hat{\mathbf{f}} = \mathbf{W}^{\mathbf{T}}(\mathbf{W}\mathbf{W}^{\mathbf{T}})^{-1}\mathbf{g}, \tag{3.8}$$

Both methods result in infeasible solutions, as shown in Figure 3.7. This occurs because the operator **W** is highly undetermined. In other words, it has more variables than equations. In addition, when a line of the operator **W** is organized in matrix form, most of its energy is concentrated in the middle of the respective crossing point, as illustrated in Figure 3.8. Thus, due to the sparse characteristic and undetermined condition in the sensitivity matrix, little information is available to increase resolution by conventional approaches.

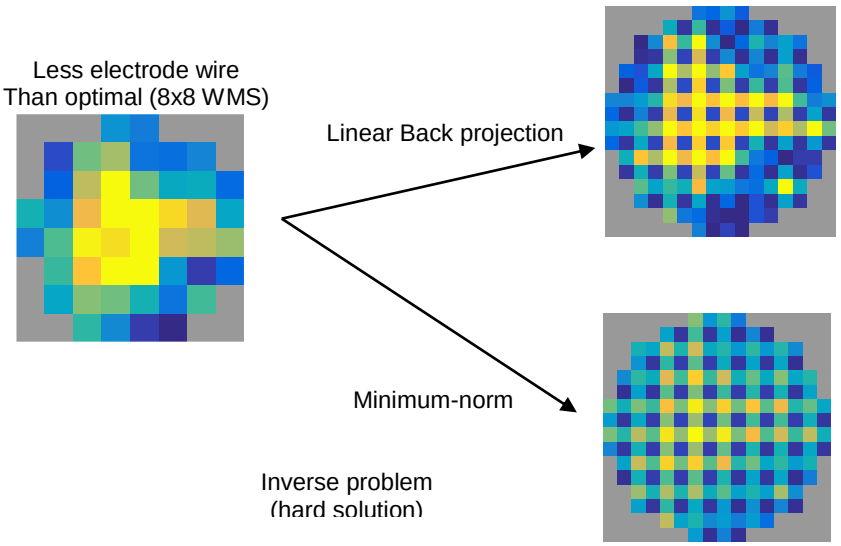

Figure 3.7: Infeasible results from conventional image reconstruction methods.

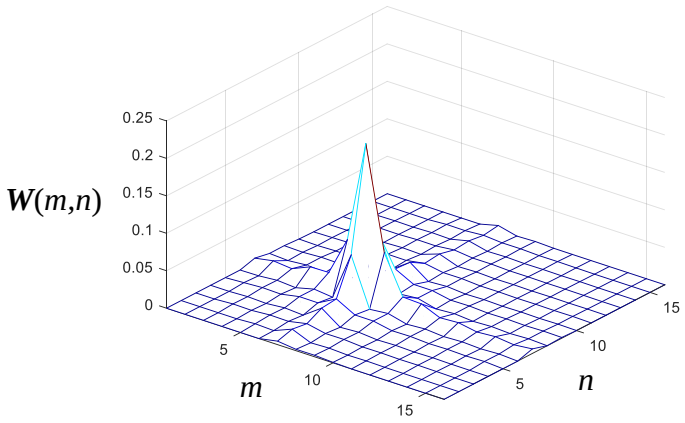

Figure 3.8: Point-Spread Function of WMS calculated by FEM.

As solution to the problem of indetermination, we used real 16x16 WMS flow data to determine a Multivariate Gaussian flow model, which was then used as regularization in the reconstruction. This approach is solved by the optimization problem known as *Maximum a posteriori* (MAP) that is described in the form:

$$\hat{\mathbf{f}}_{\mathrm{MAP}} = \boldsymbol{\mu}_{\mathbf{f}} + \boldsymbol{\Sigma}_{\mathbf{f}} \mathbf{W}^{T} (\mathbf{W} \boldsymbol{\Sigma}_{\mathbf{f}} \mathbf{W}^{T} + \lambda \mathbf{I})^{-1} (\mathbf{g} - \mathbf{W} \boldsymbol{\mu}_{\mathbf{f}}) ., \tag{3.9}$$

where, $\boldsymbol{\Sigma}_{\mathbf{f}}$ and $\boldsymbol{\mu}_{\mathbf{f}}$ are the covariance and average matrices, respectively. Both parameters are estimated by experimental data from WMS with 16x16 resolution, which are detailed in the Section 3.4.2. Results of Equation (3.9) are presented and discussed in the Chapter 4.

3.3 Experimental setup

In order to estimate the statistical parameters required in Equation (3.9) as well as to validate the method proposed, a set of experiments were carried out in a flow loop located in the NUEM at the Federal University of Technology - Paraná (UTFPR-Curitiba). The experimental loop is a test facility for transient two-phase flow (air/water). Its structure is composed by a horizontal acrylic pipe with inner diameter 26 mm and 9 m of length. The Figure 3.9 presents the schematic of the plant.

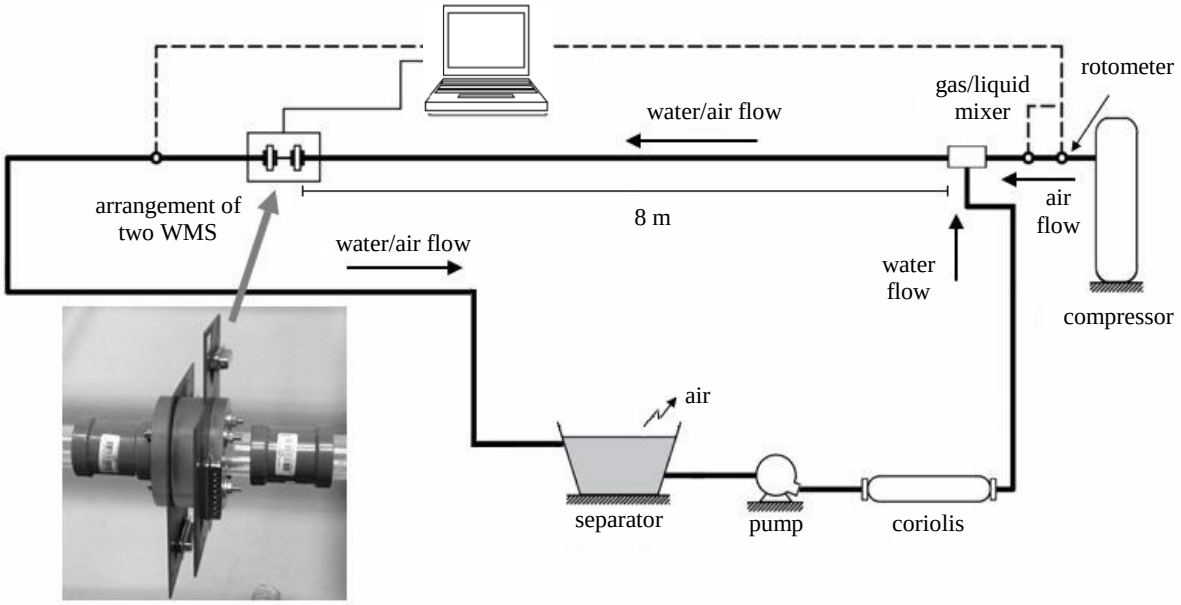

Figure 3.9: Flow loop scheme to measure two-phase flows (water-air).

The compressor and pump inject air and water, independently, into the pipe through a gas-liquid mixer. The superficial velocity of the air is controlled manually by a valve, while the water superficial velocity is controlled by a pump, which in turn is controlled by a variable frequency invertor. Values of water velocity are tuned by the software LabVIEW. The water/air mixture streams trough the long test section and then returns to the separator, where water is stored and reused and air is expelled to the atmosphere.

A Coriolis flow meter and a set of rotameters measure the velocity input of water and gas before the mixture, respectively. Setting the value of both velocities, different flow patterns of water and air mixtures can be observed and measured. This relationship was presented in Section 2.1.3b).

3.3.1 Measurement section

The measurement section is composed by an arrangement of two wire-mesh sensors spaced by an acrylic flange with thickness of 2.3 cm. The first sensor is always a 16x16 WMS used as reference (higher resolution). The second sensor is replaced for each set of experiments, assuming four resolution possibilities: 8x8, 6x6, 4x4 or 2x2 (to be reconstructed).

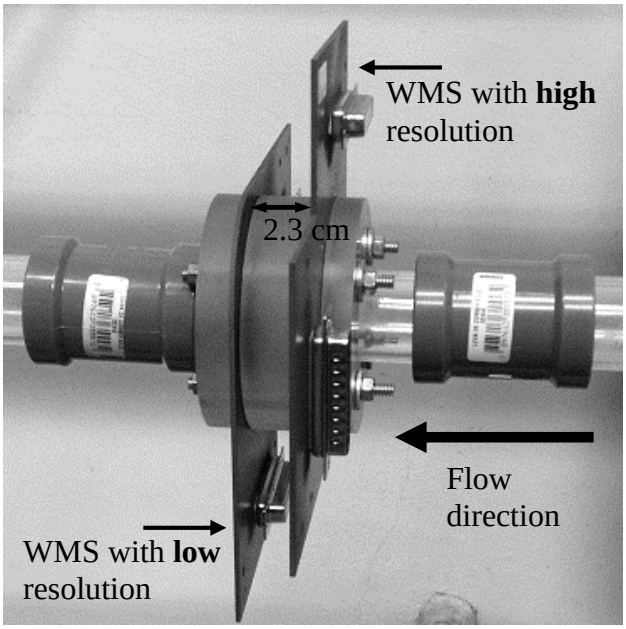

Figure 3.10: Arrangement of WMS with high and low resolution used in the experiment.

The 16x16 WMS is positioned at a distance of 8 m from the liquid/gas mixer, i.e. ~300 L/D, thus, a two-phase flow is fully developed. It is placed always first because we want avoid intrusive effects on the reference data caused by the other WMS that will be reconstructed. In this way, the reference data keeps its original confidence of measurement. The sensor with less electrode wires measures the flow perturbed by the first WMS. However, this disturbance has been neglected.

3.3.2 Wire-Mesh sensor design

All sensors used in the experimental acquisition are shown in the Figure 3.11. The WMS were manufactured using printed circuit board (PCB) technology. The electrode wires are stainless steel stretched and grooved on the PCB. The two planes of transmitter and receiver wires are axially spaced by 1.8 mm. Finally, the spacing between the electrode wires is given by the general relationship:

$$d_w = \frac{D}{N+1}, \tag{3.10}$$

where D is the pipe diameter (1 inch/ 25.4 mm) and N the number of transmitter or receiver wires.

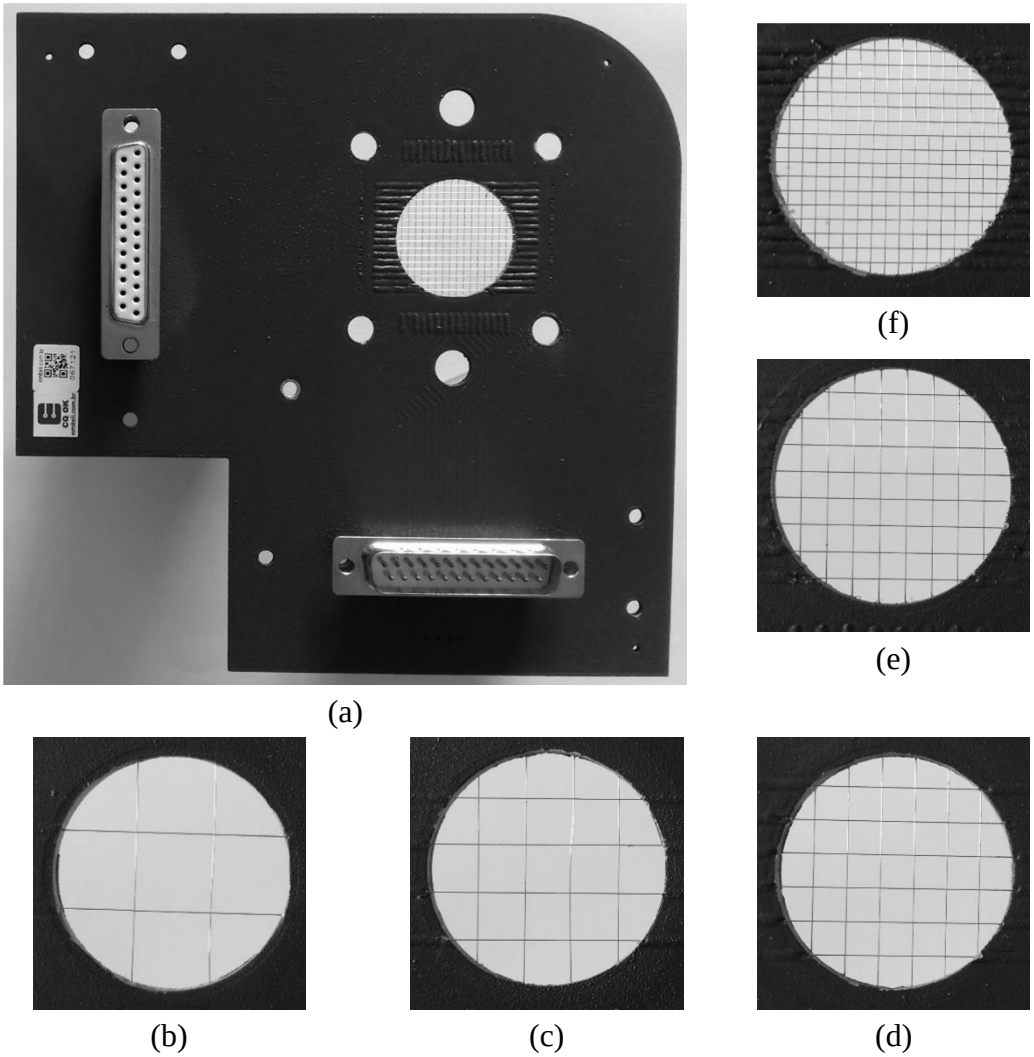

Figure 3.11: WMS manufactured and used during the experimental acquisition (a) front view of a 16x16 WMS used as reference; zoom of the electrode wires (b) 2x2 (c) 4x4 (d) 6x6 (e) 8x8 (f) 16x16.

The Table 3.3 summarizes the spatial resolution of the WMS used in this work.

Table 3.3: Spatial resolution of Wire-mesh with inner diameter of 1 inch.

16x16	8x8	6x6	4x4	2x2
1.49 mm	2.82 mm	3.63 mm	5.08 mm	8.47 mm

3.4 Experimental Data Processing

Once the experimental setup was completed, calibration data were recorded with 2 kHz sampling frequency for 60 s. The set of wire-mesh sensors were used in the capacitive mode (Da Silva, 2008). To measure the low calibration data, we removed the arrangement of sensors of the flow loop to ensure that the wires were dry. The high calibration data were measured setting a high superficial velocity of the water and keeping the gas valve closed. In this way, according to Da Silva (2008), the permittivity distribution over the cross-section can be determined as

$$\varepsilon(i,j,k) = \exp\left(\frac{V_{\log}(i,j,k) - V_L}{V_{\mathrm{H}} - V_{\mathrm{L}}}\right), \tag{3.11}$$

where, V_L and V_{H} are the voltage signals of the low and high calibration data, respectively, which are applied for every crossing point. Due to the approach of the linear relationship between the measured permittivity and phase fraction, the local phase fraction distribution can be determined in the form

$$\alpha(i,j,k) = \frac{\varepsilon_{\mathrm{H}}(i,j) - \varepsilon(i,j,k)}{\varepsilon_{\mathrm{H}}(i,j) - \varepsilon_{\mathrm{L}}(i,j)}, \tag{3.12}$$

here, the local void fraction $\alpha(i,j,k)$ is a three-dimensional matrix that is usually used for visualization of the pipe cross-section. The indexes i and j are the spatial coordinates and k the discrete-time.

The calibration procedure was carried out in the thirteen experiments (H1-H15 and A1-A4). The superficial velocity of air and water assumed different configurations as shown in the Figure 3.12. All experiments were recorded with 2 kHz sampling frequency for 60 s. The data measured by the second wire-mesh were aligned with the data of the first one due to the time delay caused by the distance between the two sensors (more details will be discussed in the next section). About 80,000 frames were used per experiment.

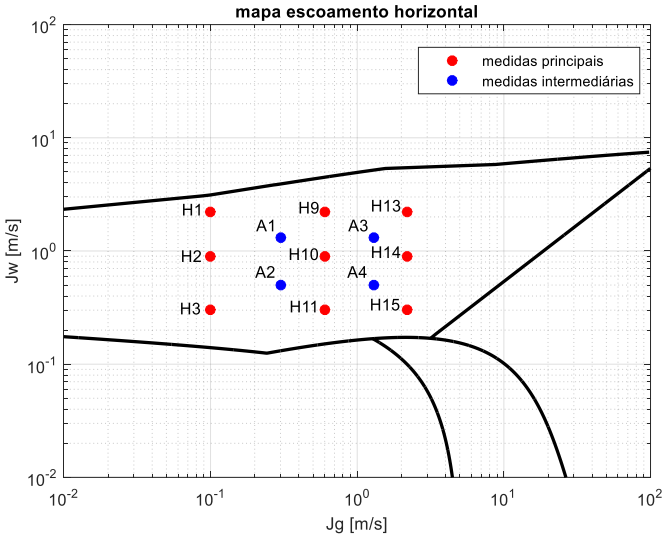

Figure 3.12: Two-phase flow map. Main (red) and auxiliary (blue) operating points, respectively.

Furthermore, each set of experiments (H*i* and A*i*) was repeated five times for a better statistical analysis. In this way, the first set of experiments (only the H*i* points) were used for two purposes: calculate the flow statistical parameters (average and covariance); and estimate the experimental sensitivity map, which was used to validate the numerical sensitivity map solved by FEM. The other four sets of experiments were employed to validate the reconstruction algorithm based on statistical approach (Equation (3.9)). The auxiliary A*i* points have not been incorporated as priori knowledge to show the efficiency of the reconstruction algorithm working far from the operating points H*i*.

3.4.1 Data Alignment

Due to the distance between the arrangement of the two sensors, the mean void fraction of both acquisition data are shifted by a time-delay τ (Figure 3.13). The alignment of the two signals is necessary to allow comparisons between reference and lower resolution/reconstructed data.

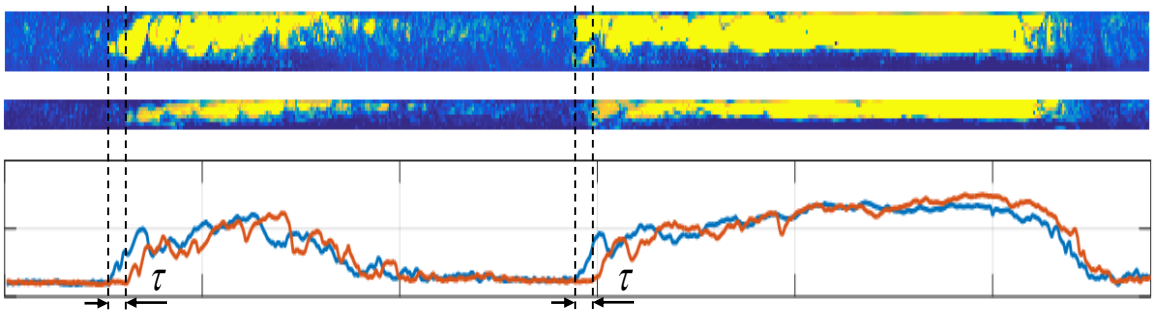

Figure 3.13: Time delay between the high- and low- resolution data. The bottom graphic is the void fraction of the both measurement.

The time delay between the two data measured is estimated by the cross-correlation method, which consists to solve the following problem:

$$\tau = \arg\max_{m} \sum_{m=-\infty}^{\infty} f[m]g[m+n] \,. \tag{3.13}$$

Here, τ is given by the point of maximum argument of the convolution $(f * g)[n]$, where f and g are the void fraction time series measured by the both sensors. The Figure 3.14 shows the signal of the cross-correlation of a typical WMS acquisition.

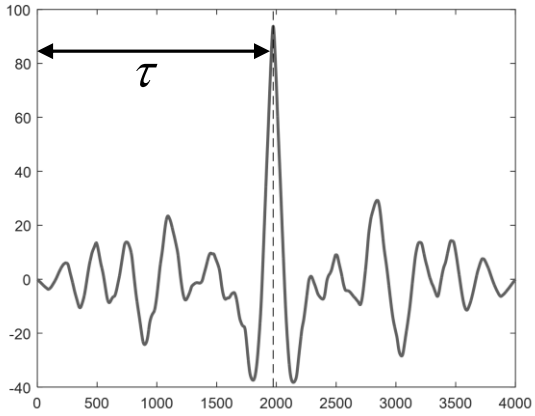

Figure 3.14: Two experimental data aligned by the cross-correlation method.

Since the time-delay is calculated, both signal can be finally aligned as the Figure 3.15.

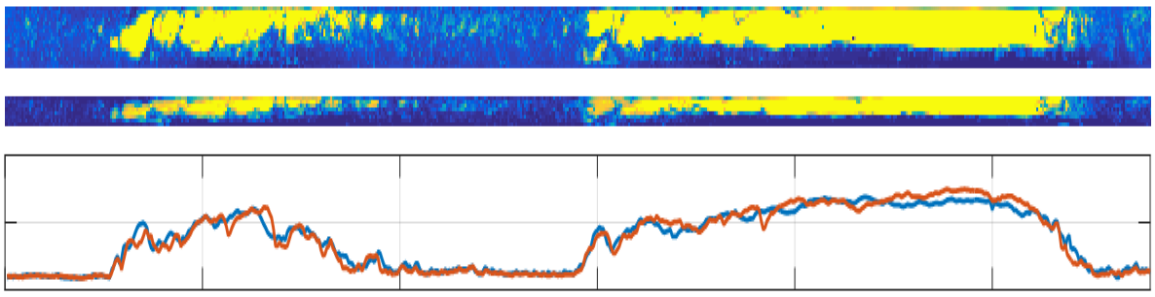

Figure 3.15: Data aligned by the cross-correlation method.

This procedure has been applied for each pair of experiments measured by the arrangement of two WMS in the present research.

3.4.2 Statistical Parameters of Two-Phase Flow

The acquisition model of WMS is undetermined when used to increase image resolution of a sensor with less than optimal electrode wires. In other words, this problem admits infinite

solutions. For this reason, *a priori* knowledge is incorporated to the cost function to limit the number of candidate solutions.

In this research, the *prior* model term is composed by statistical parameters of the two-phase flow data (average and covariance). Both parameters were calculated from the experimental flow data measured by a 16x16 WMS. Before calculating the statistical parameters, the frames of each experiment H*i* were organized as

$$\mathbf{F}_{\mathrm{H}i} = \begin{bmatrix} \mathbf{f}_{\mathrm{H}i}(j) \\ \mathbf{f}_{\mathrm{H}i}(j+1) \\ \vdots \\ \mathbf{f}_{\mathrm{H}i}(j+k) \end{bmatrix}, \quad j = 1, 2, \cdots, k. \tag{3.14}$$

where, j is the index of acquisition sample and k is the length of the window time series. The frame $\mathbf{f}_{\mathrm{H}i}$ is described in vector form and is a line of the matrix $\mathbf{F}_{\mathrm{H}i}$. Here, a single frame $\mathbf{f}$ is approximated by a Gaussian random vector, that is

$$\mathbf{f} \sim N(\boldsymbol{\mu}_{\mathbf{f}}, \boldsymbol{\Sigma}_{\mathbf{f}}). \tag{3.15}$$

where $\boldsymbol{\mu}_{\mathbf{f}}$ and $\boldsymbol{\Sigma}_{\mathbf{f}}$ are the average and covariance, respectively. In a general form, both parameters are solved by

$$\boldsymbol{\mu}_{\mathbf{X}} = \mathrm{E}(\mathbf{X}) = \frac{1}{n}\sum_{i=1}^{n}\mathbf{X}, \tag{3.16}$$

$$\boldsymbol{\Sigma}_{\mathbf{X}} = \mathrm{E}\left[\left(\mathbf{X} - \mathrm{E}[\mathbf{X}]\right)\left(\mathbf{X} - \mathrm{E}[\mathbf{X}]\right)^{\mathrm{T}}\right]. \tag{3.17}$$

Substituting the variable $\mathbf{X}$ of the equations (3.16) and (3.17) by the set of operating points of matrix (3.14), it is achieved *a priori* information used in the MAP algorithm. Here, a set of operating points were used instead of a single experiment with the goal to improve robustness of the reconstruction algorithm. Thus, different from our previous work (Dias, et al. 2016), the reconstruction algorithm is able to work far from a single operating point.

The Figure 3.16 shows the covariance and average calculated from nine experiments (H1 to H9 - Figure 3.12).

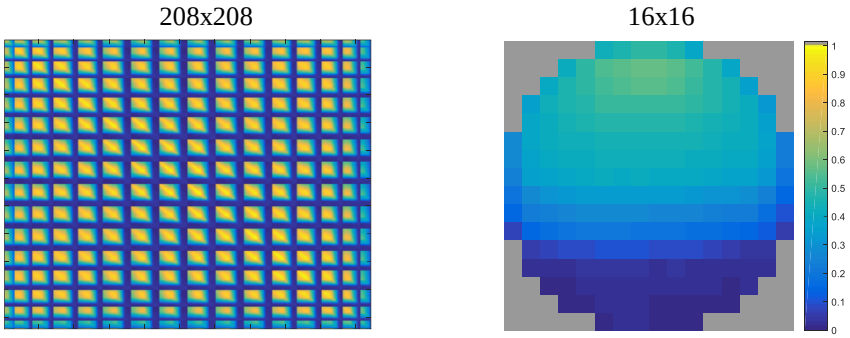

Figure 3.16: Statistical parameters extracted from a set of two-phase flow data. (a) Covariance; (b) Average.

In the next chapter, we will present experimental results of reconstruction method based on the statistical parameters shown in Figure 3.16. In this way, the maximum a posteriori (MAP) is used to increase resolution of WMS data with less electrodes wires then optimal. Thus, the multivariable Gaussian Flow Model (MGFM) (covariance and average) is employed as a regularization.

Chapter 4

Results and discussions

This Chapter presents the main experimental and numerical results of the reconstruction method proposed.

4.1 Experimental results

Acquisition data were provided simultaneously by two wire-mesh sensors in a horizontal liquid-gas flow loop. Both sensors were spaced by a distance of 2.3 cm. At the first position, it was placed a 16x16 WMS and the second was a wire-mesh with less than optimal electrode wires, i.e., 8x8, 6x6, 4x4 and 2x2. In this case, the low-resolution (LR) sensors were intercalated for each set of experiments.

Once the acquisition data were calibrated and temporally aligned by cross-correlation method (Section 3.4), image reconstruction based on inverse problem was employed to increase the low-resolution data of sensors placed in the second position to 16x16. The reconstruction method is known as Maximum *a Posteriori* (MAP) and is based on statistical approach. Statistical parameters of the operating points from H1 to H15 (Figure 3.12) were incorporated into the reconstruction algorithm *a priori*.

Average and standard deviation of void fraction will be used in the following sections as performance criterion. Here, we focus on the void fraction due to its relevance in the field of multiphase flow. Void fraction of the reconstructed method is evaluated comparing with the void fraction of the following cases: 16x16 WMS (reference), low-resolution sensors without any treatment and finally, reconstructed data by spline bi-cubic interpolation.

4.1.1 Qualitative analyses of a single operating point

MAP algorithm was applied in low-resolution data performed in the exemplary operating point H14 ($J_W = 0,9$ m/s and $J_G = 2,2$ m/s). In the Figure 4.1, we compare the void fraction of the proposed reconstruction method with the 16x16 WMS data (blue), wire-mesh sensors with low-resolution data without any treatment (red) and reconstruction method by spline interpolation (grey). Here, we empirically assumed a regularization factor $\lambda = 0.0001$. The spline method was carried out by the MATLAB function *interp2*.

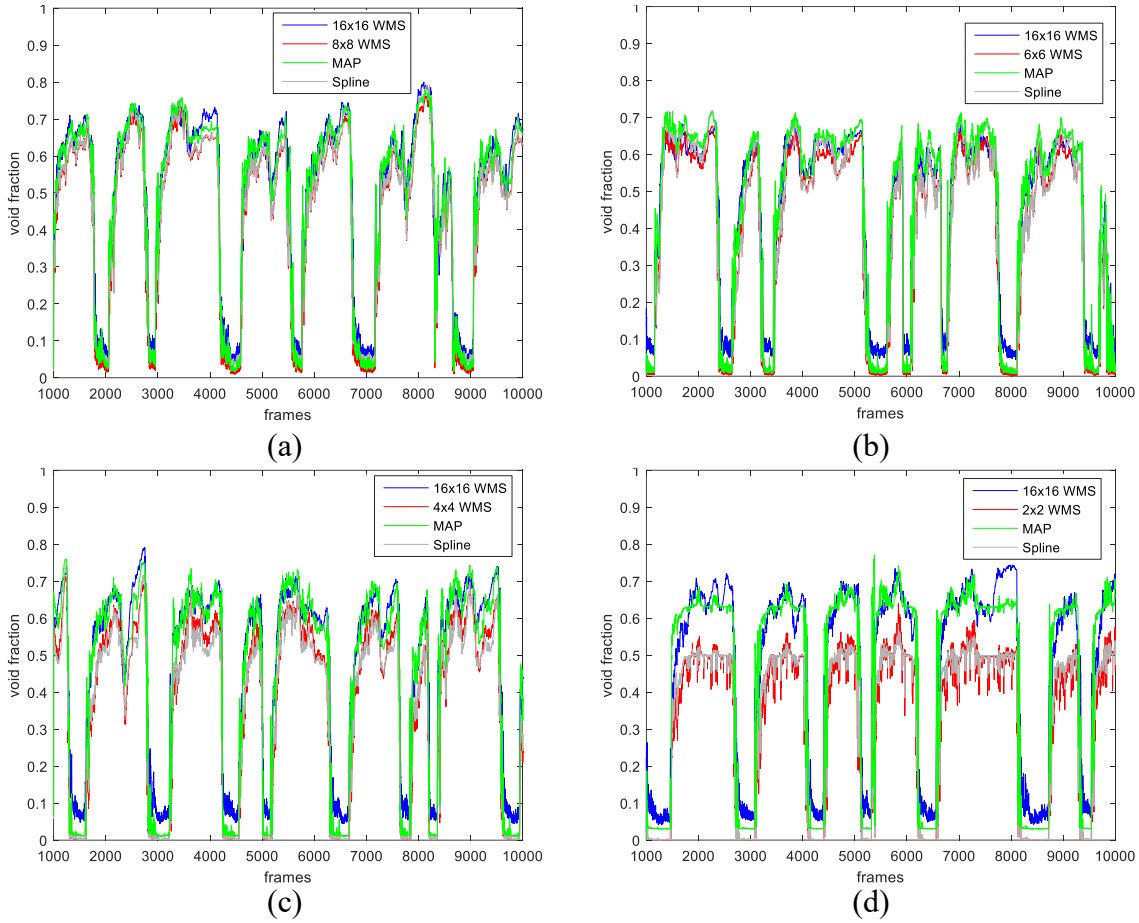

Figure 4.1: Qualitatively results of the reconstruction method in the operating point H14 for the cases: (a) 8x8 to 16x16 (b) 6x6 to 16x16 (c) 4x4 to 16x16 (d) 2x2 to 16x16. Operating point H14. Frequency sample of 2 KHz.

We can observe qualitatively from Figure 4.1 that the MAP void fraction gave satisfactory results from all four low-resolution data (8x8, 6x6, 4x4 and 2x2). This is evident especially in extremely low-resolution cases (4x4 and 2x2). Here, the void fraction distribution is almost identical with the reference (16x16 WMS), while spline interpolation gave underestimated values of void fraction as well as the WMS LR data without any treatment. For

a better analysis, MSE and RMS of the experiment from Figure 4.1 are summarized on Appendix A.

The void fraction signals shown in the Figure 4.1 can be also visualized by a virtual sectional view. This type of perspective is essential for several studies. For example, to track or estimate the volume and deformation of bubbles, analyze the void fraction distribution, etc. Figure 4.2 illustrates the virtual sectional view of the experimental data (same operating point).

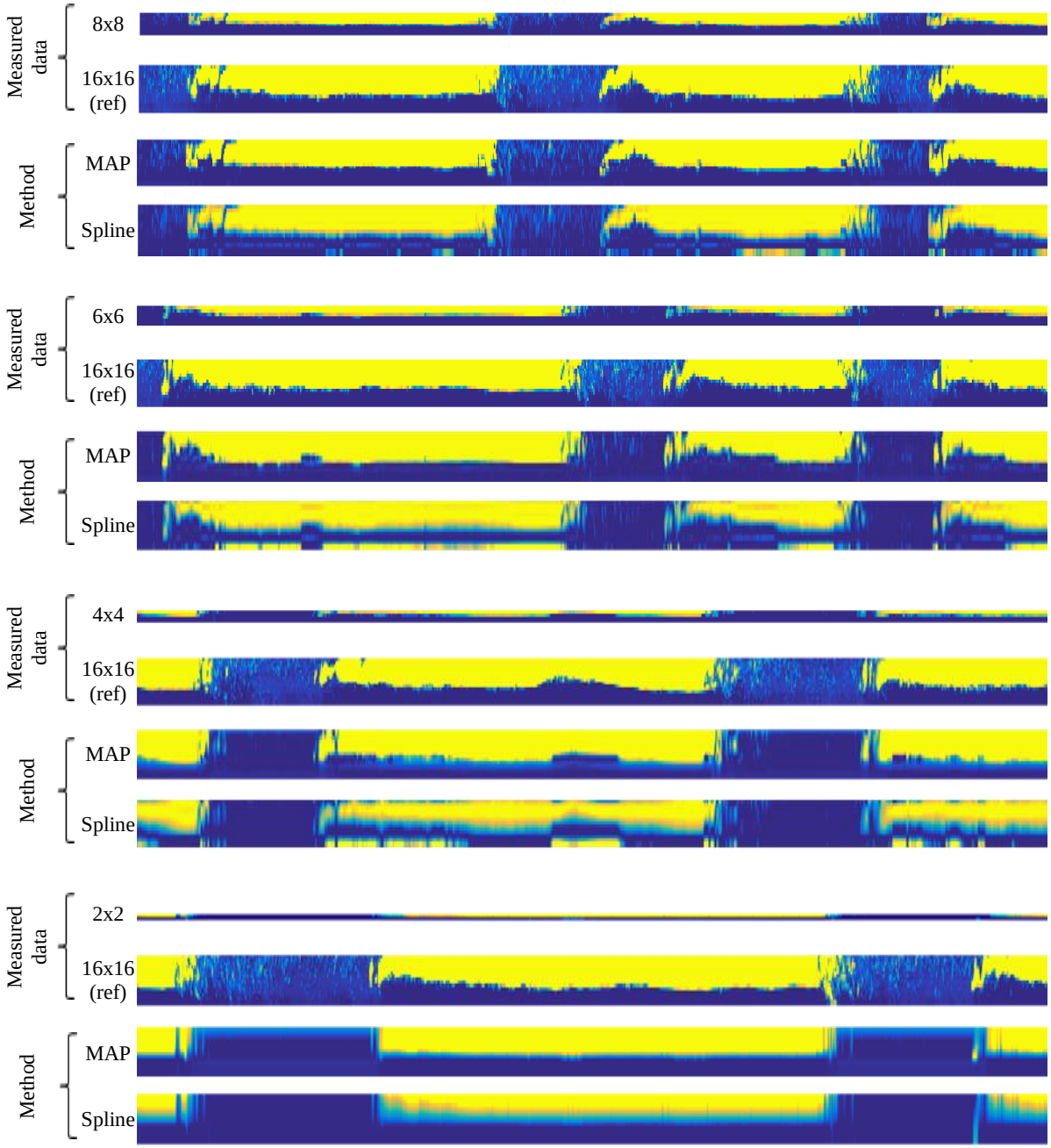

Figure 4.2: Experimental data visualization from wire-mesh sensor (Measured data). Reconstructed data visualization by maximum a posteriori (MAP) and spline interpolation. Operating point H14. Frequency sample of 2 KHz.

As shown in Figure 4.2, it is evident that MAP and spline interpolation results are similar to the reference data (16x16 WMS). However, dispersed bubbles within the liquid slug are dramatically attenuated in the resolution cases equal or less than 6x6. This occurs because the size of most of dispersed bubbles are smaller than the resolution of wire-mesh sensors data with less than optimal electrode wires and priori knowledge is not enough to recover such pixels. More evidence for this is detailed in Figure 4.3, which cross-sectional images of the pipe are depicted. Here, the frames are liquid slug chosen randomly from the experimental data in the operating point H14. In this case, low-resolution of wire-mesh sensors data with 4x4 and 2x2 electrode wires did not sense any dispersed bubble. On the other hand, the 6x6 and 8x8 WMS sensed something, but the bubbles are difficult to be reconstructed due to the poor resolution of the observed data. Therefore, reconstructed data are not exactly identical to the 16x16 WMS data

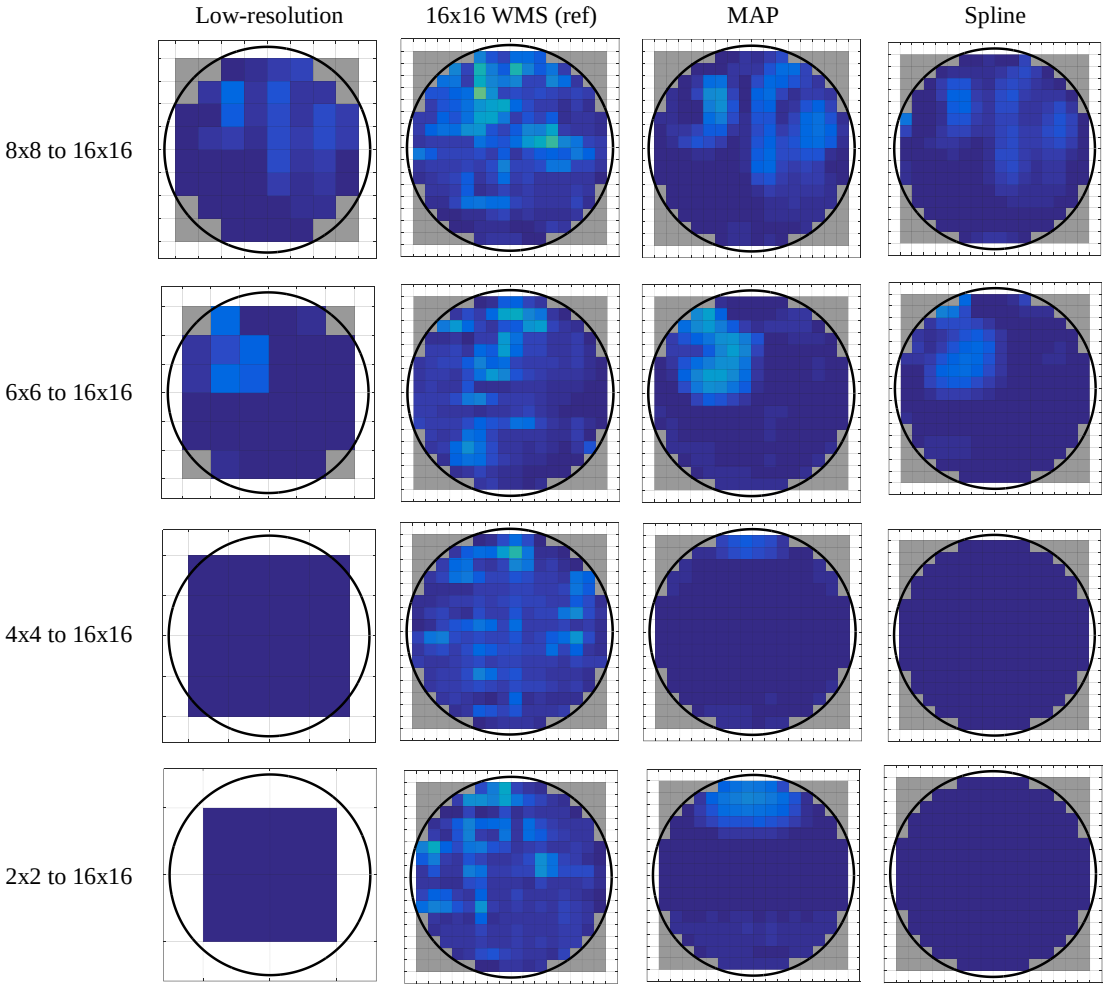

Figure 4.3: Cross-sectional images of the pipe depicting dispersed bubbles.

Returning attention to Figure 4.2, other observed point is the blurring presented in both reconstructed data. This effect is more perceptible in the spline cases, when the number of electrode wires are drastically reduced. This occurs because algorithm based on interpolation smooths the interpolated point between two extremely contrasting pixels in general. As a result, the contours between the liquid and gas phases are blurred. Figure 4.4 exemplifies this problem.

Although sometimes the blur problem does not affect the average of the cross-sectional void fraction, estimations of volume and size of bubbles may be deteriorated.

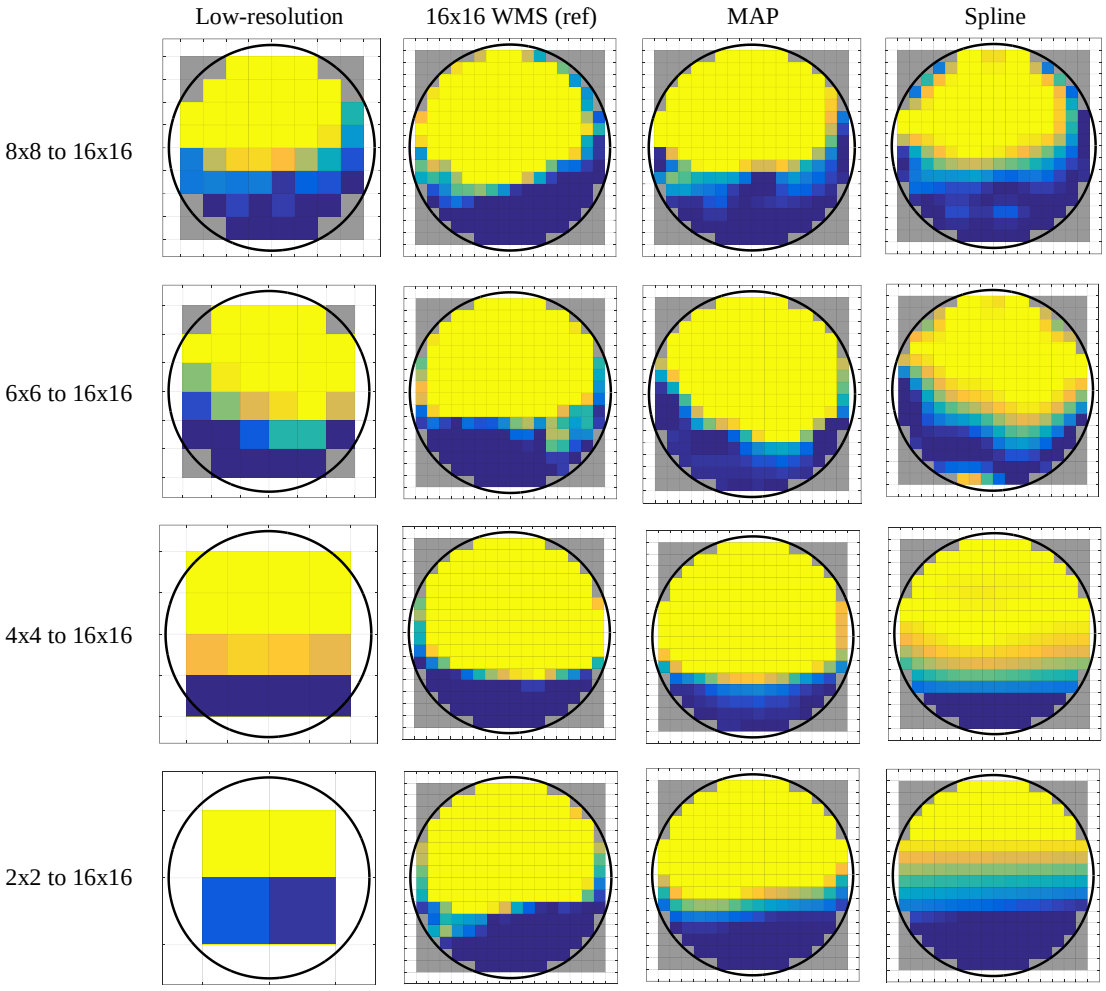

Figure 4.4: Cross-sectional images of the pipe depicting part of an elongated bubble.

4.1.2 Quantitative results

Statistical parameters were used to compare the void fraction of the reconstruction method MAP with reference from WMS low-resolution (LR) data and spline interpolation. In this way, we evaluated the MAP performance from different operating points in a global view. In this context, we defined the void fraction error as

$$\mathrm{VFE}(k) = \alpha_{ref}(k) - \alpha_{low}(k), \tag{4.1}$$

where, α_{ref} and α_{low} are the temporal void fraction measurement of the sensors with high (HR) and LR, respectively. Based on this definition, the average of the Void Fraction Error (VFE) can be described in the form

$$\overline{\mathrm{VFE}} = \frac{1}{n}\sum_{k=1}^{n}\mathrm{VFE}(k). \tag{4.2}$$

Finally, the standard deviation of the VFE is given by

$$\sigma_{\mathrm{VFE}} = \sqrt{\frac{1}{n}\sum_{k=1}^{n}\left(\mathrm{VFE}(k) - \overline{\mathrm{VFE}}\right)^2}. \tag{4.3}$$

4.1.3 Possible errors in alignment of data

Void fraction error may occur when two data are aligned by cross-correlation. For example, if a bubble deforms while passing from the 16x16 WMS to the low-resolution wire mesh sensor. Then, the sensors measure different void fraction distributions. This type of error is intensified mainly between transitions of liquid slug and elongated bubbles, i.e., in the nose and tail of the gas bubble. Unlike of the middle of the elongated bubble, which is more stable.

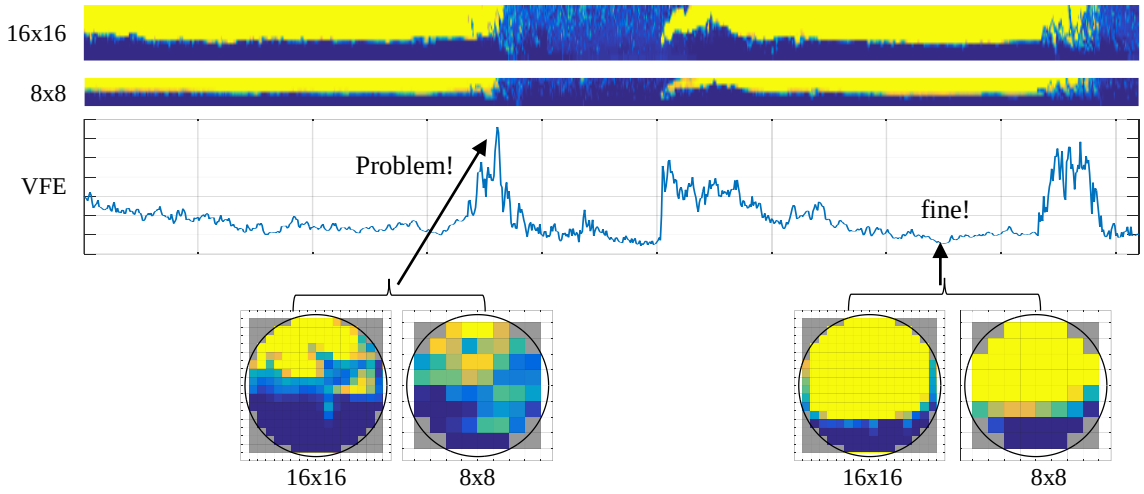

Figure 4.5: Intensification of void fraction error due the transition between tail of bubble and liquid slug. Cross-sectional images of aligned data measured by two WMS spaced by a distance of 2.3 cm.

Due to this type of error, it is reasonable to avoid the evaluation of single frames between such transitions. Therefore, the deviation of the proposed reconstruction algorithm will be calculated by the Equations (4.2) and (4.3) through large time series flow data.

4.1.4 Deviation of all operating points

All reconstruction method (MAP and Spline) and WMS low-resolution data without treatment (LRDWT) were compared from void fraction deviation (VFD). As a rule of thumb, wire-mesh sensor with optimal number of electrode wires has uncertainty of 10%. For this reason, we assumed a range of $\pm$10% to evaluate void fraction deviation (Nuryadin, Ignaczak, & Lucas, 2015). As can be seen in Figure 4.6, MAP reconstruction (blue) gave predominantly better results than spline interpolation (green) and LRDWT (red). Since VFD from MAP algorithm is into the range of 10% in the majority of operating points, while LRDWT and spline presented very poor results mainly from the 4x4 and 2x2 cases.

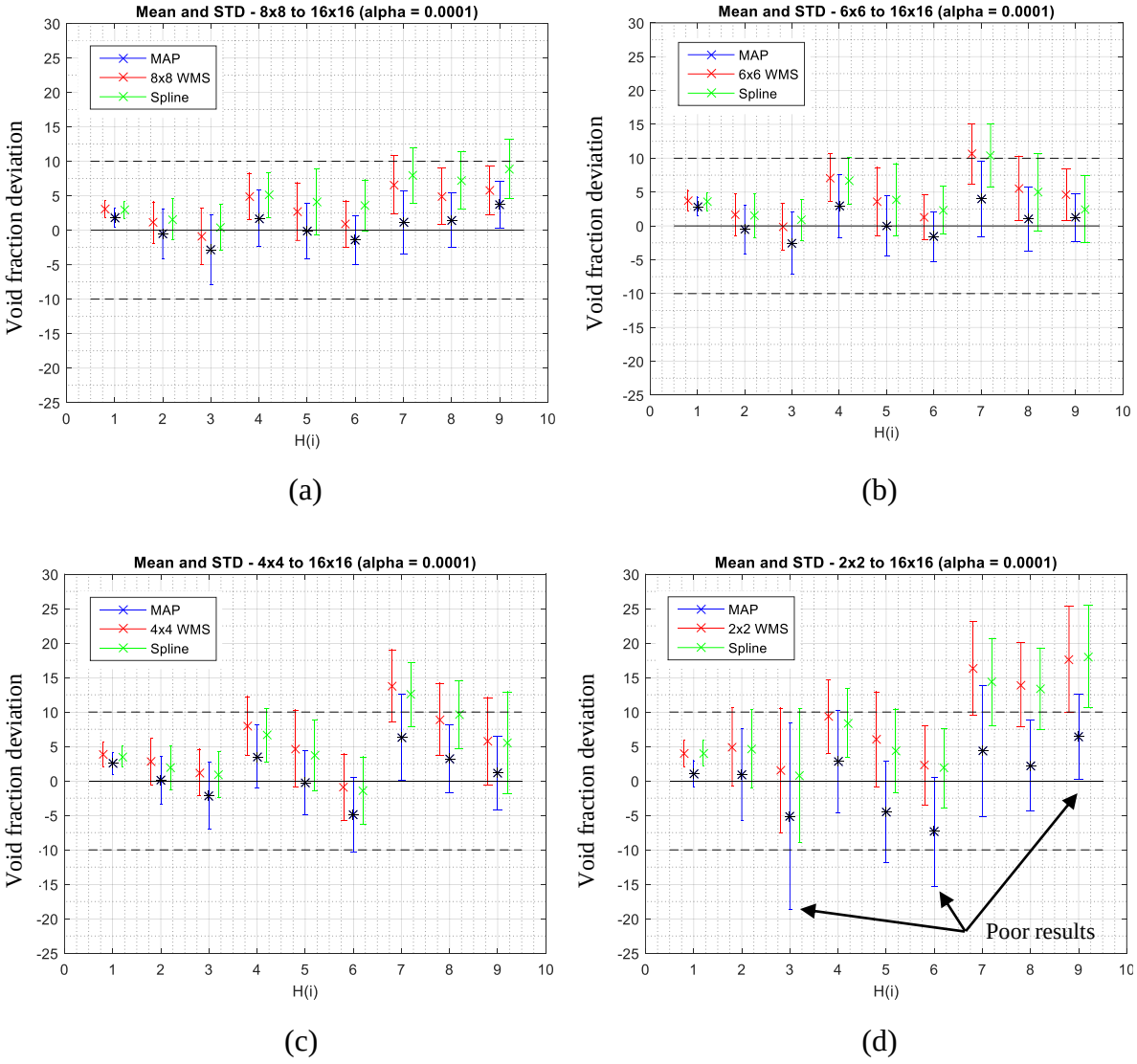

Figure 4.6: Void fraction deviation. Dashed line represents deviation into a range of $\pm$ 10%. Each figure is based on the resolution: (a) 8x8 (b) 6x6 (c) 4x4 (d) 2x2. Experiments performed with 76000 frames for each operating point in a frequency sample of 2 KHz.

We can observe from Figure 4.6 (d) (case 2x2) that VFD of some operating points are very poor when reconstructed by MAP. In particular, H3, H11, and H15. A common point between them is the low superficial velocity of water (Figure 4.7). It may suggest that MAP does not work efficiently for low rate of water velocity or that the regularization is not well tuned, since we used a single λ = 0.0001 for all cases. Other possibility is that the WMS LR data could not provide sufficient information to recover data. In other words, a single multivariable Gaussian model (MVM) as regularization is not enough to solve the indetermination problem of 2x2 cases.

Further work is planned to investigate solutions to improve such critical operating points. For example, using a specific MGFM for each different regions of the two-phase flow pattern map. Maybe one direction is to develop a cost function able to automatically choose the best regularization model for each case.

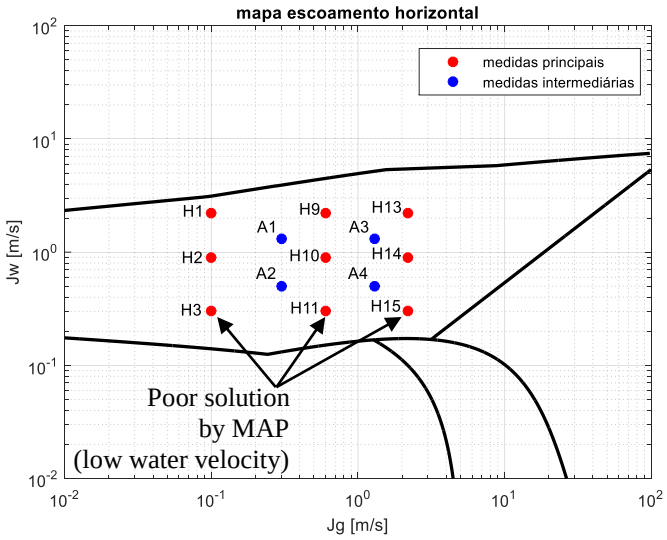

Figure 4.7: Horizontal two-phase flow map. Operating points

4.2 Towards simulation-based parameter estimation

According to Bertola (2003), experiments are essential to evaluate the performance and limitation of mathematical and numerical models. In addition, they can be a first step to better understanding of physical phenomena. In this way, we still do not have pretention to formulate theory or mathematical model based on experimental data or results presented previously. Here, our goal is to detail a way to simulate data acquisition from WMS model by FEM and compare such synthetic acquisition with real data qualitatively.

Based on the numerical model presented in Section 3.2, we removed all divisions of its sensitivity area. Then, we used a geometric form of ellipsoid to simulate elongated bubble. The model is illustrated in Figure 4.8.

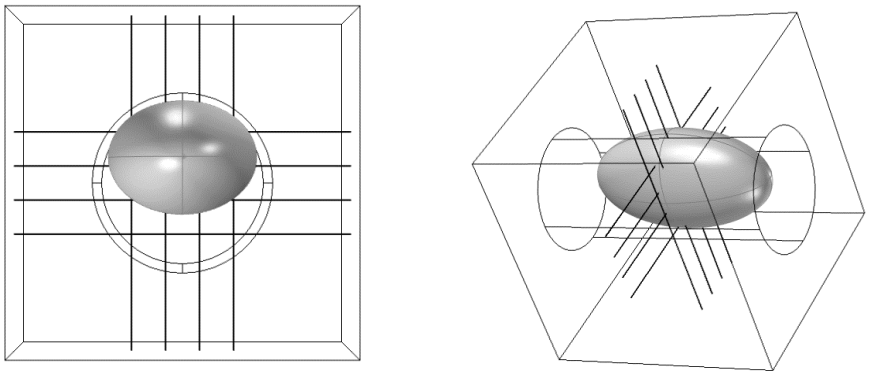

Figure 4.8: Numerical acquisition model of 4x4 WMS by FEM. Ellipsoid geometry to simulate elongated bubbles.

Using the same procedure detailed in Chapter 3, capacitance of crossing points from numerical models of 16x16 and 4x4 WMS were simulated and 30 dB noise was added to them. Then, MAP algorithm and spline interpolation were applied in the synthetic data. Finally, in order to compare synthetic and experimental data, we selected randomly two experimental frames similar to the numerical simulation. As we can see from Figure 4.9, synthetic and experimental data are in good agreement in the case of the enlarged bubble. In this way, numerical models based on FEM might be used to try new reconstruction algorithms without the need of experimental data.

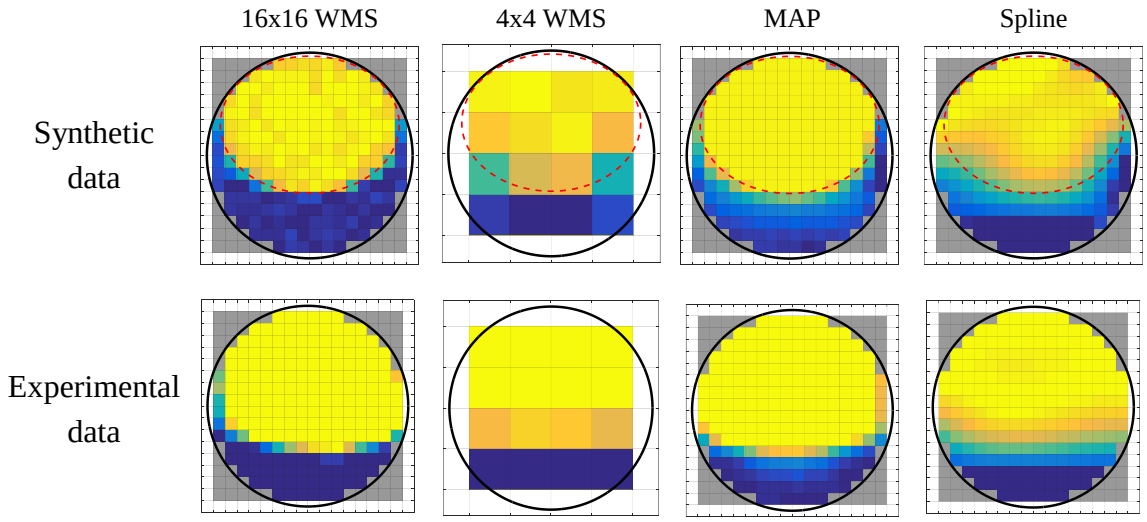

Figure 4.9: Qualitative comparison between synthetic and experimental data.

Chapter 5
Conclusion

This last Chapter summarizes the main achievements and limitations of the reconstruction method proposed as well as further works.

5.1 Conclusions

Prior works have presented image reconstruction method based on inverse problems to increase resolution of wire-mesh sensor with optimal number of electrode wires. Conventional reconstruction techniques, such as linear back projection have been successfully applied for this purpose. However, conventional algorithms gave very poor results when used to increase resolution of wire-mesh sensor data with less than optimal number electrode wires. Inadequate solution are found because the sensitivity map is highly undetermined.

In order to solve the indetermination problem, use used in the present study a reconstruction algorithm based on statistical approach. Thus, we assumed a multivariable Gaussian flow Model, which has analytic solution by solving the optimization problem known as Maximum a Posteriori (MAP). Real 16x16 WMS flow data were incorporated to the model and used as regularization. In this way, we found that MAP is able to increase resolution of WMS data satisfactory, even in the cases where the observation data had very low-resolution, e.g. from resolution data of 4x4 and 2x2 to 16x16. Here, experimental results showed that MAP provides less blur in the reconstructed image than spline interpolation when the number of electrode wires of WMFS is reduced. In addition, void fraction deviation of MAP gave into the range of 10% in the majority of the cases, even using non-optimal regularization parameters. Therefore, this study indicates that the reconstruction method proposed is appropriated.

The main limitation of this approach is the need of experimental data to find multivariable Gaussian models. In future works, the numerical model by finite element method should be improved to find such statistical parameters.

5.2 Further works

The following points are open:

- Extending the reconstruction method based on MAP for other two-phase flow patterns.
- Testing the algorithm with experimental data from different pipe diameter, with the goal to find a relationship between the diameters.
- Generate prior knowledge from synthetic data using FEM or equivalent as well as formulate a mathematical model that describe the prior information.
- Formulate a cost function to optimize the choice of the best multivariate Gaussian model and λ in a given operating point.

Appendix A

In order to evaluate the quality of the results presented in the Section 4.1.1, we used the Mean Squared Error (MSE) and Root Mean Square (RMS). Both indexes are defined as follows:

$$\mathrm{MSE}(\hat{\mathbf{f}}) = \frac{1}{n}\sum_{i=1}^{n}(\hat{\mathbf{f}}_i - \mathbf{f}_i)^2, \tag{A.1}$$

$$\mathrm{RMS}(\hat{\mathbf{f}}) = \sqrt{\frac{1}{n}\sum_{i=1}^{n}(\hat{\mathbf{f}}_i - \mathbf{f}_i)^2} = \sqrt{\mathrm{MSE}(\hat{\mathbf{f}})}. \tag{A.2}$$

The following tables present the MSE and RMS of the MAP algorithm, spline interpolation and low resolution data (LR) without no treatment, where the high resolution data (HR) is the "true" value. Qualitative results of this experiment is discussed in the Section 4.1.1.

As expected, the MAP algorithm performs better than spline interpolation and LR data.

Table A.1: Mean Squarer error (MSE) of the reconstruction method in the operating point H14. Frequency sample of 2 KHz. 15985 number of frames.

	8x8	6x6	4x4	2x2
MAP	0.0018	0.0023	0.0035	0.0047
Spline	0.0073	0.0057	0.0128	0.0206
LR	0.0042	0.0055	0.0113	0.0225

Table A.2: Root Mean Squarer (RMS) of the reconstruction method in the operating point H14. Frequency sample of 2 KHz. 15985 number of frames.

	8x8	6x6	4x4	2x2
MAP	0.0423	0.0481	0.0595	0.0683
Spline	0.0854	0.0756	0.1132	0.1435
LR	0.0650	0.0742	0.1062	0.1501

References

Azzopardi, B. (2006). *Gas-liquid Flows.* New York: Begell House.

Bertola, V. (2003). *Modelling and Experimentation in Two-Phase Flow* (1 Ausg.). Springer-Verlag Wien.

Bovik, A. C. (2000). *Handbook of Image and Video Processing.* Academic Press.

Da Silva, M. J. (2008). *Impedance Sensors for Fast Multiphase Flow Measurement and Imaging.*

Dias, F. A., Pipa, D. R., & Da Silva, M. J. (2016). Increasing Resolution of Wire-Mesh Sensor Data using Statistical Reconstruction Approach. *8th World Congress on Industrial Process Tomography.*

Dos Santos, E. N., Vendruscolo, T. P., Morales, R. E., Schleicher, E., Hampel, U., & Da Silva, M. J. (2015). Dual-modality wire-mesh sensor for the visualization of three-phase flows. *Measurement Science and Technology, 26(10)*, 105302.

Falcone, G., Hewitt, G. F., Alimonti, C., & Harrison, B. (2002). Multiphase Flow Metering: Current Trends and Future Developments. *Journal of Petroleum Technology*, 77-84.

Falcone, G., Hewitt, G., & Alimonti, C. (2009). *Multiphase flow metering: principles and applications* (Vol. Vol. 54). Elsevier.

Kay, S. M. (1993). *Fundamentals of statistical signal processing: Estimation theory.* Prentice Hall.

Libert, N. (2013). Sistema de Medição Capacitivo para Determinação da Fração de Vazio em Escoamentos Bifásicos. *Dissertação - Programa de Pós-Graduação em Engenharia Elétrica e Informática Industrial, Universidade Tecnológica Federal do Paraná*, 115. Curitiba.

Measurement, N. S. (2005). Handbook of Multiphase Flow Metering. *Revision 2*.

Nuryadin, S., Ignaczak, M., & Lucas, D. (2015). On the accuracy of wire-mesh sensors in dependence of bubble sizes and liquid flow rates. *Experimental Thermal and Fluid Science, 65*, 73-81.

Park, S. C., Park, M. K., & Kang, M. G. (2003). Super-resolution image reconstruction: a technical overview. *IEEE signal processing magazine, 20(3)*, 21-36.

Prasser, H. M. (2008). Novel experimental measuring techniques required to provide data for CFD validation. *Nuclear Engineering and Design, 238(3)*, 744-770.

Prasser, H. M., Böttger, A., & Zschau, J. (1998). A new electrode-mesh tomograph for gas–liquid flows. *Flow measurement and instrumentation, 9(2)*, 111-119.

Sun, Q., & Wang, H. (2011). Mesh Wire Tomography combined with a modified sensitivity map. *IEEE International Conference*, (S. 74-78).

Taitel, Y., & Dukler, A. E. (1976). A model for predicting flow regime transitions in horizontal and near horizontal gas-liquid flow. *AIChE Journal*, 47-55.

Thiele, S., & Hampel, U. (2010). CapWMS 1.1 - User Manual. 32. Forschungszentrum Dresden Rossendorf.

Unser, M. (1999). Splines: A perfect fit for signal and image processing. *IEEE Signal processing magazine, 16(6)*, 22-38.

Unser, M. (2000). Sampling-50 years after Shannon. *Proceedings of the IEEE, 88(4)*, 569-587.

WAGNER, M., DA SILVA, M. J., THIELE , S., & HAMPEL , U. (2008). Simulation-based investigation of spatial sensitivity distribution of wire-mesh sensors. *Proceedings of Comsol Comference.*

Weimin, L., Li, Y., & Peng, L. (2016). Sensitivity map based sub-pixel image reconstruction by using simulation data for capacitive wire-mesh tomography. *8th World Congress on Industrial Process Tomography.*